Ore Geology Reviews 161 (2023) 105670

Contents lists available at ScienceDirect

Ore Geology Reviews

journal homepage: www.elsevier.com/locate/oregeorev

Distribution and enrichment mechanism of critical metals in the Danping bauxite deposit, northern Guizhou (SW China)

Hailan Li [a,b,c], Hongpeng Fan [b,*], Jie Zhang [a,d,*], Zhilong Huang [b], Can Jiang [c], Lin Ye [b], Lin Wu [b,e]

[a] College of Resource and Environmental Engineering, Guizhou University, Guiyang 550025, China
[b] State Key Laboratory of Ore Deposit Geochemistry, Institute of Geochemistry, Chinese Academy of Sciences, Guiyang 550081, China
[c] Panzhihua University, Panzhihua 617000, China
[d] Mining College, Guizhou University, Guiyang 550025, China
[e] Guizhou Provincial Coalfield Geology Bureau, Guiyang 550025, China

ARTICLE INFO

Keywords:
Karst bauxite
Critical metals
Lithium
Rare earth elements
Enrichment

ABSTRACT

Critical metals are indispensable for the global scientific and economic development, and their shortage has drawn attention to critical metal exploration in bauxite-related rocks. Bauxite deposits, especially karst-type ones, are usually enriched in critical metals like Li and REE (rare-earth elements La-Lu and Y). In this study, we analyzed the bauxite ore-bearing rocks at Danping (Guizhou, SW China) with a combination of XRF, ICP-MS, XRD, and SEM-EDS techniques, with the aims to investigate the distribution characteristics and enrichment mechanisms of the critical metals (e.g., Li, Ga, Zr, Sc, and REE). The bauxite ore layer at Danping is unconformably contacted with the underlying Huanglong Formation (Fm.) limestone or the Hanjiadian Fm. mudstone/shale, and the overlying Qixia Fm. limestone or Liangshan Fm. carbonaceous shale. Lithium is mainly enriched in the top and bottom of the bauxitic clay strata (abbrev. OBC and UBC, respectively). Gallium is enriched in all the bauxite layers, OBC and UBC. Zirconium is moderately enriched in the bauxite layer, whilst Sc is more enriched in the UBC and its nearby wallrocks (e.g., compact bauxite). REE are locally enriched in/around the basement, with the total REE content of the bauxite ore host being 33.3 to 3082 ppm. In situ analysis indicates that the bauxite-bearing rocks contain REE minerals, including bastnasite and xenotime. Moderate to strong lateritization likely plays a vital role in the different enrichments of critical metals, especially in the bauxite and kaolinitic bauxite zone. Physicochemical conditions of the mineralization are very complex. The Li enrichment may have been closely linked to the clay formation and enrichment, especially during the pre-lateritization and late-leaching stages. REE are mainly enriched in the lateritization stage, and then percolated downward via acidic leaching, where differentiation and re-enrichment occur. When REE migrate to an alkaline environment (caused by Huanglong Fm. limestone), bastnaesite precipitated readily, eventually forming REE-rich claystone and concentrated along the alkaline barrier of carbonate rock.

1. Introduction

Bauxite deposits have been generally divided as laterite bauxite and karst bauxite (Bárdossy, 1982; Chen et al., 2022). Karstic bauxite represents 14% of world bauxite resources, and its ore-bearing rock series are commonly enriched in metals which are critical to modern technological development (Mameli et al., 2007). Consequently, the value of bauxite ore has increased with the limited supply of such metals (Vidal et al., 2013; Mongelli et al., 2016; Huang and Fan, 2022). China is rich in bauxite resource (5th in the world) with mainly of them are karst type (Du et al., 2022; Ling et al., 2020; Wang et al., 2013a). The northern Guizhou area, belonging to the East Asian metallogenic belt, is an important bauxite region with many large-scale karst bauxite deposits (Bardossy and Aleva, 1990; Huang et al., 2014). Recent studies revealed that the bauxite-bearing rock series in this area are supernormal enrich in metals such as Li, Ga, Zr, Sc, and REE (rare-earth elements La-Lu and Y), that has the potential for comprehensive utilization (e.g., Huang and Fan, 2022). So far, little is known about host minerals and mode of

* Corresponding authors at: College of Resource and Environmental Engineering, Guizhou University, Guiyang 550025, China (J. Zhang).
E-mail addresses: fanhongpeng@vip.gyig.ac.cn (H. Fan), jzhang@gzu.edu.cn (J. Zhang).

https://doi.org/10.1016/j.oregeorev.2023.105670
Received 28 February 2023; Received in revised form 9 September 2023; Accepted 12 September 2023
Available online 14 September 2023

occurrence of these metals in the bauxite-bearing rock series in northern Guizhou, which, however, are critical to assess the economic potential of bauxite deposits.

Bauxites in northern Guizhou occur in the Lower Permian Dazhuyuan Formation (Fm.), and mainly deposited in continental shore and lacustrine environment (Han et al., 2016; Jin et al., 2018). Paleoclimate was mainly tropical-subtropical hot and humid. The depositional environment was mainly oxidizing and locally anoxic (Chen et al., 2022; Jin et al., 2018; Wang et al., 2023; Xu et al., 2017). Previous studies on the northern Guizhou bauxite deposits were mainly dedicated to the ore deposit characteristics and genesis (Chen et al., 2022; Jin et al., 2018; Lei et al., 2023; Ling et al., 2023; Zhou et al., 2022), mineralization environment (Chen et al., 2022; Yu et al., 2019) and age and ore-material sources (Gu et al., 2013a; Gu et al., 2013b; Xu et al., 2017).

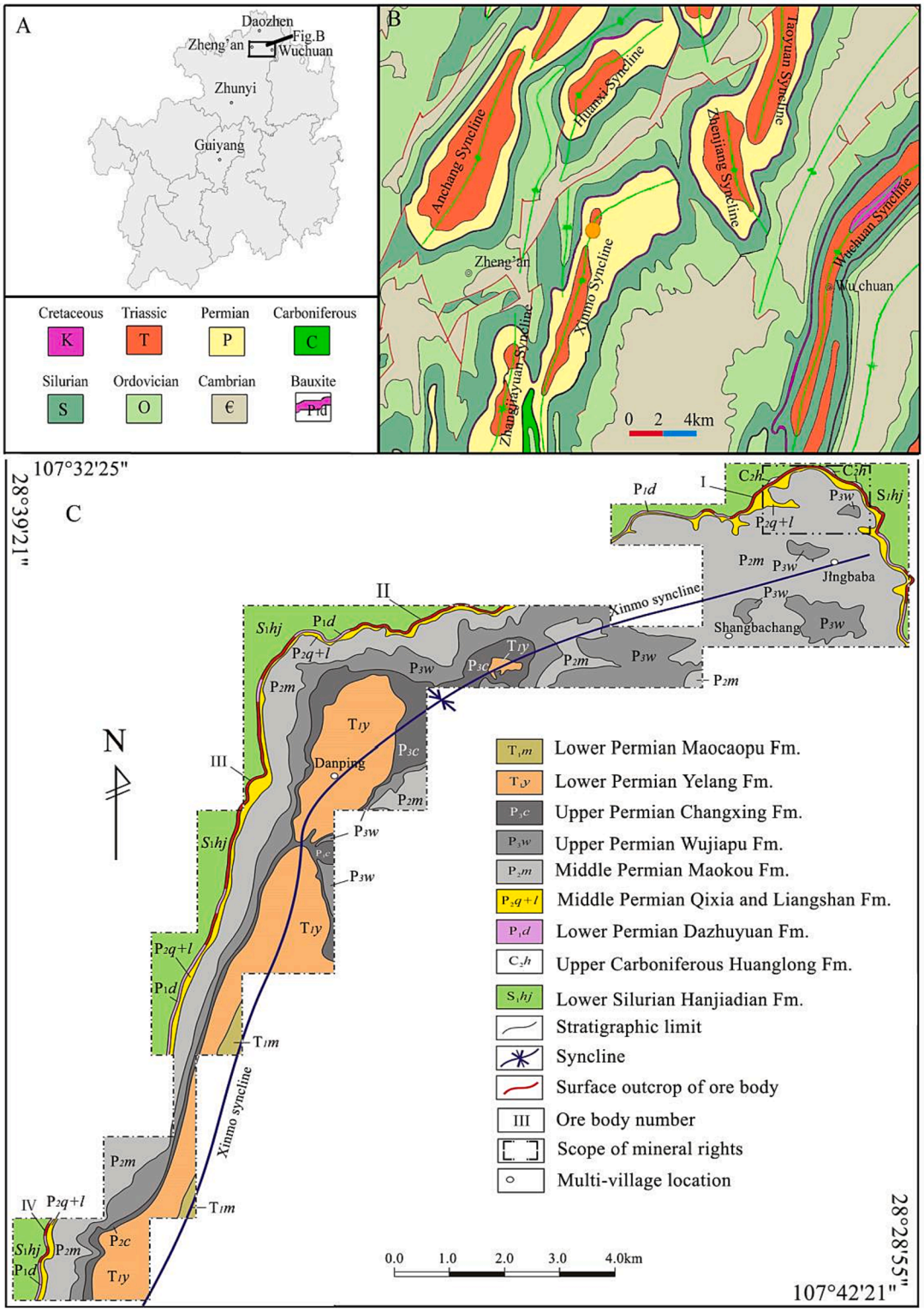

Fig. 1. (A) Map showing the location of Guizhou, China; (B) Geological map showing the location of Danping; (C) Geological map for the Danping bauxite deposit in northern Guizhou (Jin et al., 2019).

Research on the associated critical metals in these Al-bearing rocks is inadequate, especially concerning the enrichment mechanism of critical metals. The large Danping deposit is a typical karst type bauxite deposit in northern Guizhou (Fig. 1). It contains an estimated billion tonnes of bauxite ore @ 58 wt% Al_2O_3 (Xu et al., 2017). Especially, the deposit is featured by significant enrichment of critical metals (Li, Ga, Zr, Sc and REE). In this study, we analyzed the occurrence, migration and enrichment of these critical metals in the Danping bauxite through a combination of petrologic, mineralogical and geochemical analysis. The results will provide a basis for further study of critical metals in karst-type bauxite.

2. Geological background

2.1. District geology

The northern Guizhou area is located in the southwestern part of the Yangtze Block. The bauxite in northern Guizhou is an important part of the South Chongqing-Central Guizhou bauxite belt (Gu et al., 2013b; Huang et al., 2014). The region received prolonged sedimentation from the Cambrian to the Middle Miocene, forming extensive and thick layers of Al-rich silicate rocks, which represent the source rock for bauxite (Chen et al., 2022; Huang et al., 2014). By the Late Silurian-Late Carboniferous, the sea-level may have dropped to expose the Hanjiadian Fm., which then underwent strong weathering and denudation (Yu et al., 2019; Zhou et al., 2022). By the Early Permian-Middle Permian, the Hanjiadian Fm. was uplifted, and again subjected to strong lateritic weathering under warm and humid conditions, forming the bauxite deposits in northern Guizhou (Gu et al., 2013b; Li et al., 2020). Paleomagnetic data suggest that the region was in the tropics (8°-14°S) during the Carboniferous, whose warm humid climate favors the formation of bauxite (Yu et al., 2019; Zhou et al., 2022). The ore host at northern Guizhou may have undergone several uplifting events after the diagenesis. This may have formed the current topography of the bauxite deposits in northern Guizhou, featured by decreasing elevation from north to south.

The major structures in northern Guizhou are NNE-trending reverse faults, primarily formed in the anticlinal axis and the two limbs (Jin et al., 2015). The Lower Permian Dazhuyuan Fm. bauxite ore host is covered by the Liangshan Fm. carbonaceous shale or the Qixia Fm. tuffs. The ore host overlies mainly on the Lower Silurian Hanjiadian Fm. mudstone/shale, and locally (including Danping) on the erosional surface of the Carboniferous Huanglong Fm. limestone (Li et al., 2020). Local exposed strata include Cambrian to Lower Silurian and Upper Carboniferous to Triassic ones, which are locally covered by Quaternary sediments (Gu et al., 2013b; Huang et al., 2014). Distribution of the major bauxite deposits is controlled by the N-/NE-trending Yanshanian (Jurassic-Cretaceous) orogeny-related synclines (Gu et al., 2013b); Fig. 1).

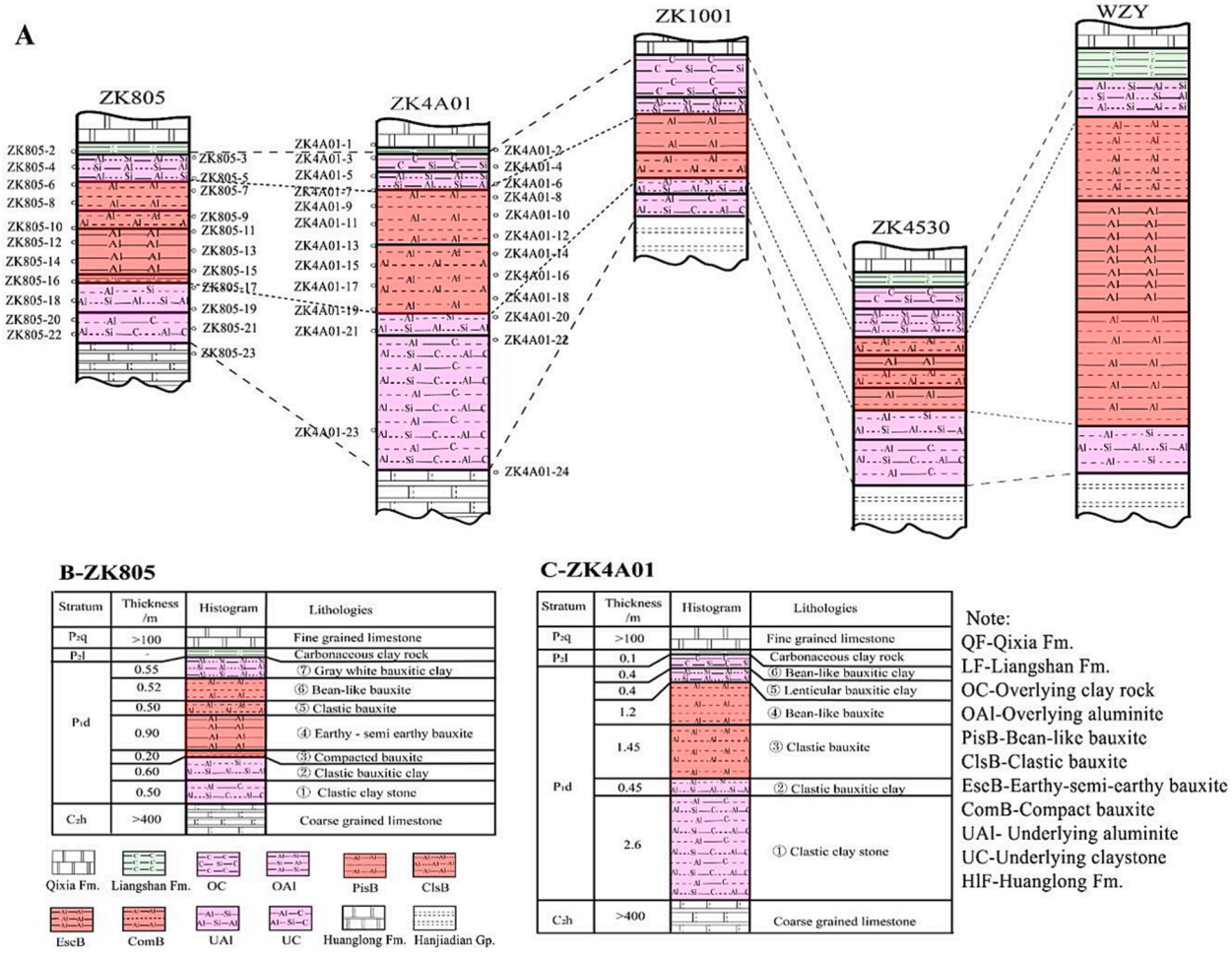

Fig. 2. Distribution and stratigraphy of ore-host sequence at Danping. (A) Correlation of the ore-host thickness; (B) ZK805 stratigraphic columns of ore-host series; (C) ZK4A01 stratigraphic columns of ore-host series. QF-Qixia Fm, LF-Liangshan Fm, OC-Overlying clay rock, OAl-Overlying aluminite, PisB-Bean-like bauxite, ClsB-Clastic bauxite, EseB-Earthy-semi-earthy bauxite, ComB-Compact bauxite, UAl- Underlying aluminite, UC-Underlying claystone, HlF-Huanglong Fm.

2.2. Local geology

The Danping bauxite is located in Wuchan-Zheng'an-Daozhen (WZD) karst-type bauxite belt in northern Guizhou with a total length of nearly 120 km. The mining rights area is about 40 km and 3.0 m-10 m thick. The bauxite-bearing rock series contained in this area belong to the Lower Permian Dazhuyuan Fm. (P_1d), distributed around the Xinmo Syncline, with an estimated bauxite resource of 2228.91 Mt and an Al_2O_3 grade of 45.83 wt%-70.82 wt% (Xu et al., 2017). Except for the absence of the middle and upper Silurian, Devonian and Carboniferous systems, the mine area is developed to varying degrees from the Lower Silurian Hanjiadian Fm. to the Lower Triassic Maocaopu Fm. (Fig. 1). The bauxite deposits mainly unconformably overlie the mudstone/shale surface of the Lower Silurian Hanjiadian Fm. or the limestone erosional surface of the Carboniferous Huanglong Fm. (Figs. 1 and 2). The geological structure of the study area is relatively simple, and the main fold structural framework is a new type of syncline with asymmetric wings, axial plane facing west, and overall inclination towards south.

Based on mineralogy, facies and textural changes, seven and six distinct layers or horizons for ZK805 and ZK4A01, from bottom to top, are recognized for the typical bauxite profiles (Figs. 2 and 3). The geological profile ZK805 (total thickness 3.77 m) measured in this study is representative of the ore-host characteristics of the mine, and comprises seven layers from the bottom to top (Fig. 2B):

① claystone layer (avg. 0.50 m thick): grey-black colored, with occasional small amounts of yellowish debris, dominated by siliceous and

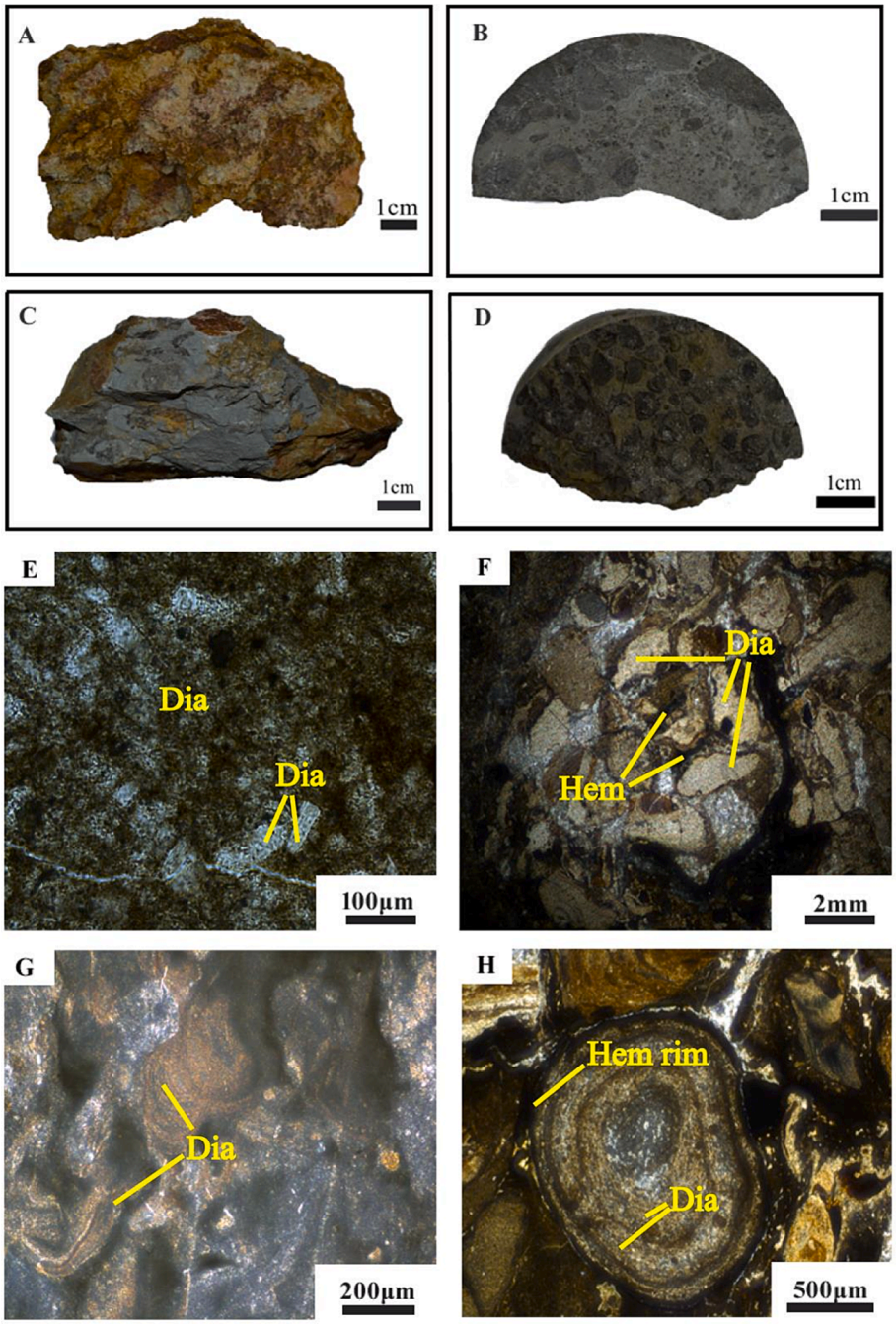

Fig. 3. Hand-specimen photos. (A) Earthy and semi-earthy bauxite, (B) Clastic bauxite, (C) Compact bauxite, (D) Bean-like bauxite, (E) Diaspore with good crystallinity and gelatinous diaspore in earthy and semi-earthy bauxite, (F) Cementation of diaspore and hematite in the matrix, (G) Gelatinous diaspore, (H) Concentric annular layers of diaspore oolite. Abbreviations: Dia-Diaspore, Hem-Hematite.

carbonaceous clastic clay stone.

② upper minor ore host (avg. 0.60 m thick): gray – gray black colored, dominated by clastic bauxitic clay. It consists mainly of kaolinite, chlorite, and illite, with minor diaspore, goethite, and hematite.

③–⑥ major ore host separated by lithologic difference (avg. 2.12 m thick): gray – gray black colored, dominated by (semi-)earthy bauxite (EseB), clastic bauxite (ClsB), compacted bauxite (ComB), and bean-like bauxite (PisB; Figs. 2 and 3). The ore host is composed mainly of diaspore, with minor boehmite and trace gibbsite and cliachite. Other trace minerals include clay minerals (kaolinite and chlorite, with rare illite and smectite), quartz, feldspar, calcite, anatase, limonite, hematite, pyrite, rutile, and zircon.

⑦ lower minor ore host (avg. 0.55 m thick): grey-white colored, dominated by bauxitic clay. It consists mainly of kaolinite, chlorite, and illite, with minor diaspore, goethite, hematite, and calcite.

The bauxite bodies are layered. Based on mineralogy, facies, and textural changes, the four types of bauxites are as follow (Figs. 2 and 3): (Semi-)earthy bauxite (Fig. 3A and E) is off-white to light yellow, loose texture, generally located in the upper part of the ore host near the oxide zone surface, and represents the best quality bauxite at Danping. Clastic bauxite (Fig. 3B and F) is dark gray to brown, with massive cryptocrystalline and agglomerate structure, distributed in all parts of the ore host. The clasts are sub-angular/-rounded, sand-dominated, and vary in size. Compact bauxite (Fig. 3C and G) is dark gray to brown, dense and hard, granular/lamellar, massive microcrystalline or cryptocrystalline, mainly located at the ore layer bottom, and represents low-quality ore. Bean-like bauxite (Fig. 3D and H) is dark brown to red, massive, mainly distributed at the ore layer top, with bean (size >2 mm) and oolite (size <2 mm), and represents low-quality ore.

3. Samples and analysis methods

Across the two boreholes at Danping in the Xinmo syncline (Figs. 1 and 2), a total of 46 samples (22 from ZK805 and 24 from ZK4A01) were collected according to lithological variations, i.e., Qixia Fm. limestone → Liangshan Fm. carbonaceous shale → Dazhuyuan Fm. bauxite ore host → Huanglong Fm. limestone for mineralogical and geochemical analyses. Whole-rock samples were crushed and grinded to <0.074 μm. XRF (X-ray fluorescence spectrometry) fusion and solution ICP-MS (inductively coupled plasma mass spectrometry) were used to determine the major and trace element contents, respectively. Mineralogical studies were performed by optical microscopy, SEM-EDS (scanning electron microscopy-energy spectroscopy), and XRD (X-ray diffraction). All the analyses were performed at State Key Lab of Ore Deposit Geochemistry, Institute of Geochemistry, Chinese Academy of Sciences.

Major element contents were measured on a PANalytical AXIOS-PW4400XRF, with a precision of better than 5%. 0.7000±0.0005 g of the sample was weighed and placed in a platinum crucible, then 7.0000 ±0.0005 g of the composite flux ($Li_2B_4O_7$: $LiBO_2$: LiF = 4.5: 1: 0.4) was added and mix thoroughly. The mixture was melted in a furnace (1150 °C) to form glass discs, which were then analyzed by XRF. Trace element contents were determined on a Plasma Quant-MS Elit ICP-MS. The powdered samples (50 mg) were dissolved in high-pressure Teflon bombs for 48 h at ~195 °C using HF and HNO_3. The solution was prepared in a specific ratio and Rh was used as the internal standard to monitor signal drift (Qi et al., 2000). The international standards GBPG-1 and OU-6 and the Chinese national standard AGV-2 were used for data quality control, which yielded better than 10% accuracy.

XRD was used to quantify the mineral compositions, and was conducted on randomly-oriented powder specimens with a D/MAX-2000 diffractometer. The analysis used Cu Kα (λ = 1.5406 Å) radiation at 56 kV voltage and 182 mA current. Polished sections were prepared from representative samples for the SEM-EDS analysis. SEM analyses were done on an EPMA-1600 SEM using Genesis EDAX. BSE (back-scattered electron) images were obtained at 120 kV accelerating voltage and ~10 μA beam current.

4. Results

4.1. Petrography and mineralogy

Optical microscopy, XRD, and SEM analyses show that the bauxite ore minerals at Danping are mainly diaspore and minor boehmite, whilst the gangue minerals include mainly Ti-bearing minerals (anatase and rutile), sulfides (pyrite and chalcopyrite), and Al-silicates (kaolinite, chlorite, smectite, and muscovite). In addition, trace zircon, calcite, quartz, feldspar, limonite, dolomite, and calcite were also identified (Fig. 4A – D, Fig. 5).

The bauxitic clay (abbrev. OBC (including OC and OAl) and UBC (including UAl and UC), respectively)) comprises primarily kaolinite, anatase, chlorite, rutile, boehmite, chalcopyrite, pyrite, and diaspore (Fig. 4E – G, Fig. 5). Fine-grained xenotime (YPO_4) is distributed sporadically in the bauxite layer (Fig. 4A and B), and Ce-bearing parisite ($Ce_2Ca(CO_3)_3F_2$) is present in the bauxite clay at the bottom of the bauxite profile (Fig. 4E and G).

4.2. Major and trace element geochemistry

4.2.1. Major element compositions

The bauxite ore at Danping has 46.44–74.48 wt% Al_2O_3 and 3.86–25.28 wt% SiO_2 (A/S ratio = 1.84 to 19.3), and 1.03–17.99 wt% Fe_2O_3 and 2.18–3.91 wt% TiO_2. It also contains minor (<6 wt%) MgO, Na_2O, K_2O, MnO, and P_2O_5. The (semi-) earthy bauxite ore has considerably higher Al_2O_3 content (68.06–74.48 wt%) than the other three type of ores (Al_2O_3 = 46.44–67.67 wt%).

The bauxitic clay (including OBC and UBC) has lower Al_2O_3 than the bauxite ore, with the OBC and UBC having Al_2O_3 of 35.34–44.73 wt% and 29.82–44.02 wt%, respectively. The OBC and UBC have SiO_2 = 26.85–38.84 wt% and 33.18–42.01 wt%, Fe_2O_3 = 2.70–10.36 wt% and 2.12–14.34 wt%, and TiO_2 = 1.80–2.47 wt% and 1.45–2.07 wt%, respectively (Table 1).

The ternary Al_2O_3-SiO_2-Fe_2O_3 plot is widely used to indicate weathering trends, such as lateritization and aluminization (Schellmann, 1986; Wang et al., 2013b), in which the Danping bauxite samples fall along a trend from being Si-rich to being Al-rich (Fig. 6). This shows that the bauxite, bauxitic clay, and carbonaceous claystone have undergone strong, moderate, and weak lateritization, respectively, which is further confirmed by the rock assemblage that changed from bauxitic clay, bean-like, clastic/compact bauxite, to (semi-) earthy bauxite as shown in Fig. 6. Moreover, this evolutional trend is roughly consistent with the SiO_2, Al_2O_3, and Fe_2O_3 variation patterns during the bauxite formation in a typical profile of the well-studied Xinmin deposit which is another large bauxite deposit in northern Guizhou (Huang et al., 2014).

4.2.2. Trace element contents

Alkali and alkaline earth metals.

They have a wide content range, e.g., Li content w(Li) = 4.79–1540 ppm, w(Ba) = 5.44–205 ppm. The contents of Li, Be, Rb, Cs, Sr, and Ba in BC are higher than those in the bauxite (Fig. 7), and those in the (semi-) earthy ores are the lowest. The BC layer has w(Li) = 205–1440 ppm, while the compact bauxite adjacent to UAl has w(Li) = 1450 ppm. The bean-like and clastic bauxite have similar w(Li) of 12.5–204 ppm and 8.11–143 ppm, respectively, while w(Li) of the (semi-)earthy bauxite is much lower (4.79–10.6 ppm), suggesting that Li was only enriched in the early bauxite formation stages. Compared to the Clark value ((Hans Wedepohl, 1995); Fig. 7), BC and its adjacent compact bauxite in the ore host have high Li content, with an enrichment coefficient (abbreviation

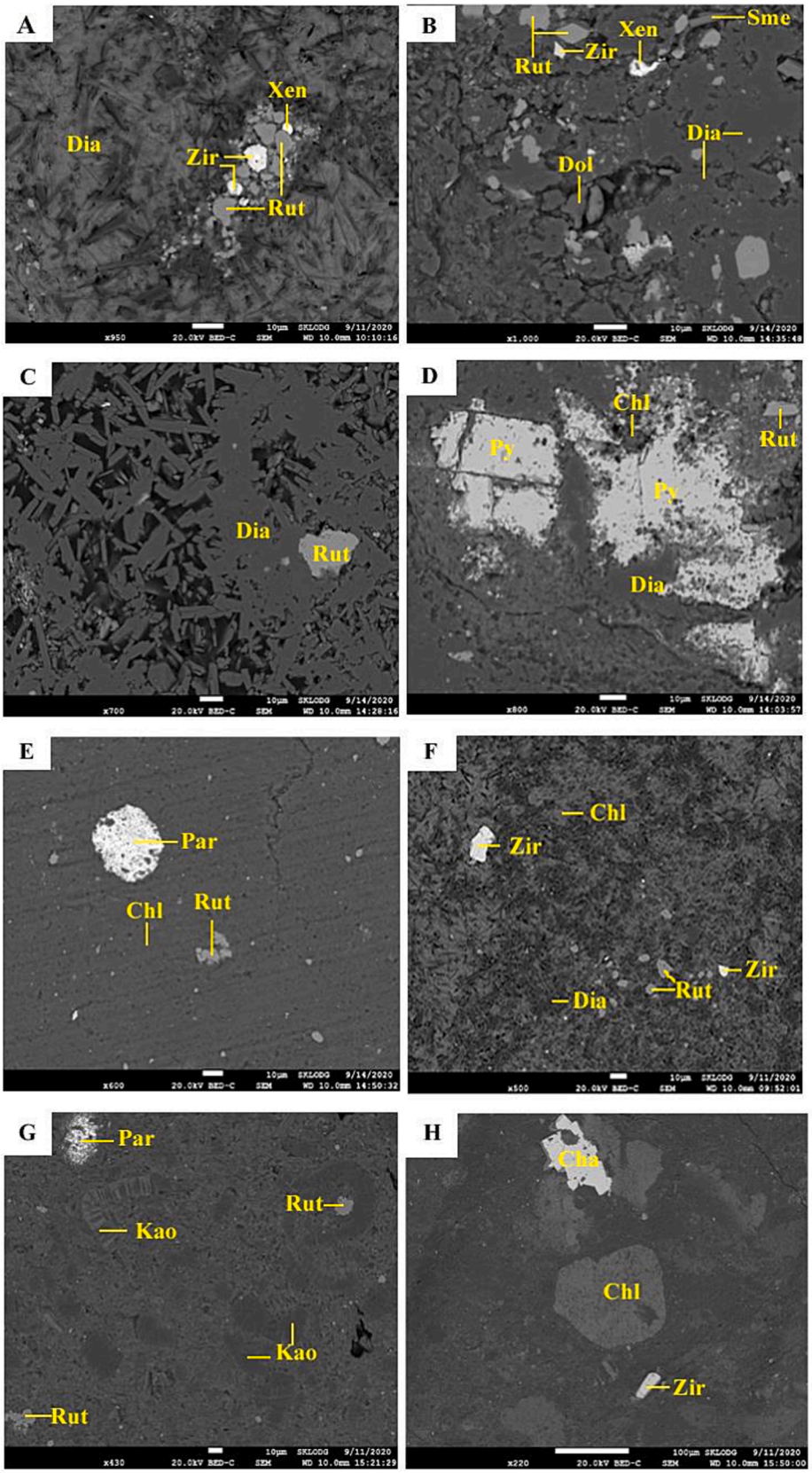

Fig. 4. BSE images: (A-D) rutile, zircon, xenotime, smectite, dolomite, and pyrite in diaspore. (E-H) parisite, rutile, zircon, diaspore, and chalcopyrite in chlorite and kaolinite. Abbreviations: Sme-Smectite, Rut-Rutile, Zir-Zircon, Kao-Kaolinite, Xen-Xenotime, Dia-Diaspore, Dol-Dolomite, Py-Pyrite, Chl-Chlorite, Par-Parisite, Cha-Chalcopyrite.

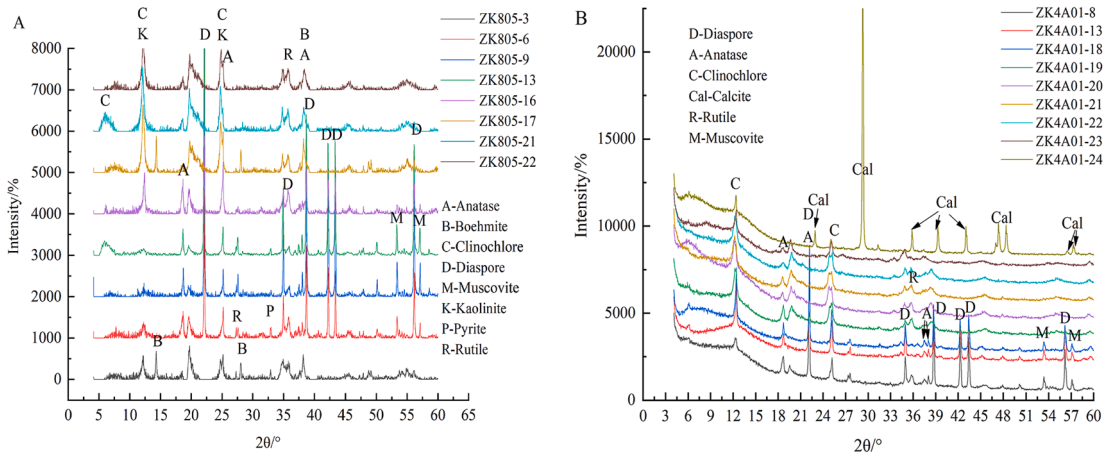

Fig. 5. XRD patterns of different ores or rocks. (A) ZK805, (B)ZK4A01.

EC, measured value/Clark value) of 0.39 to 85.56. Most of alkali and alkaline earth elements are below the Clark value, with EC of mostly below 2.42.

4.3. Transition metals and chalcophile elements

The ore host has w(Sc) = 6.62–60.6 ppm, and the compact bauxite has the highest w(Sc) (60.6 ppm) with EC of 3.79. The V, Cr, and Zn contents fall within the same order of magnitude, e.g., w(V) = 157–774 ppm. The Co, Ni, and Cu contents are relatively high, e.g., w(Co) = 2.48–69.00 ppm and w(Ni) = 3.04–238 ppm. Fig. 7 shows that the V-Cr contents of the ore host are slightly higher than those of the Clark value, with the EC mostly between 0.99 and 4.62. In contrast, the contents of most other transition metals are relatively low.

The contents of chalcophile elements (except for Pb and Mo) fall within a narrow range (within an order of magnitude), e.g., w(As) = 1.65–94.3 ppm, w(Sn) = 7.79–17.7 ppm, and w(Bi) = 0.125–1.87 ppm. The Pb (4.42–185 ppm) and Mo (0.444–10.8 ppm) contents vary widely. Contents of these chalcophile elements (except for Pb and Mo) are significantly higher than the Clark values in the ore host, with EC of 3.33–5.94 for W, 3.81–13.41 for Bi, 2.19–9.37 for Sb, and 3.77–7.52 for Sn. The ore host has EC (for Pb) = 0.54 to 4.96, and ClsB has EC = 0.54. The ore host has EC (for Mo) = 0.59 to 5.00, except for UC (0.59) and UAl (0.75; Fig. 7).

4.4. Rare metals

The ore host has varying Zr content, with w(Zr) = 371 to 1299 ppm, whilst the concentration range for other rare metals are relatively narrow, e.g., w(Nb) = 34.1–92.4 ppm and w(Th) = 21.2–64.4 ppm. The ore host has good linear Zr vs. Hf and Nb vs. Ta correlations, which implies similar activity pattern of rare metals during the bauxite formation (Fig. 8).

The rare metal contents of the ore host are higher than the Clark value, with EC = 1.88 to 3.24. Except for Th, the EC values of rare metals follow the same trend as Al_2O_3 content, showing an increase from clay stone/rock to aluminous clay to bauxite. The Th content in the ore host is high in OC, OAl, PisB, and ComB and low for the other rock types (Fig. 7).

The content of precious and rare metals (Ag, Ga, Ge, Cd, Tl, In) in the ore host are 0.030 to 57.4 ppm. Except for Tl (0.030 to 1.46 ppm), the content of other rare metals varies in narrow range, e.g., w(Ga) = 23.7 to 57.4 ppm and w(In) = 0.163 to 0.397 ppm.

Compared with the Clark value (Fig. 7), the Ag, Ga, Cd, and In contents are significantly higher, with EC = 17.10 to 34.86, 2.05 to 3.73, 2.80 to 11.11, and 3.45 to 7.94, respectively. The Ge and Tl contents are much lower, with EC = 0.36 to 2.56 and 0.16 to 1.23, respectively.

4.5. Rare earth elements (REE)

Compared with the Clark value (Fig. 7), the LREE (La-Eu) content of the claystone UC is slightly higher than the Clark value, with EC mostly of 1 to 5. Most of the bauxitic clay UAl is also locally REE enriched, with EC = 0.51 to 3.99. In particular, La and Ce are also enriched in UAl and UC (EC = 1–6). The LREE content of the overlying claystone, bauxitic clay, and bauxite in the middle/upper parts of the sequence is low, and the EC is mainly of 0.07 to 0.86. HREE (Gd-Lu-Y) of the ore host are slightly enriched relative to the Clark value (EC = 1–5).

The chondrite-normalized REE patterns (Fig. 9) shows that the profile from top to bottom (OC → UC) underwent a similar formation process. The ore host is similarly LREE enriched, with $(La/Yb)_N$ = 0.15 to 25.36 and $(La/Sm)_N$ = 0.56 to 7.02. HREE enrichment is relatively similar, with $(Gd/Yb)_N$ = 0.28 to 2.28. This shows that the ore host has undergone similar degree of weathering and leaching (Maksimovic and Pantó, 1991).

Compared to chondrite, ∑La-Nd is significantly enriched relative to ∑Sm-Dy and ∑Ho-Lu, ∑Sm-Dy is moderately-slightly enriched relative to the other two, and the ∑Ho-Lu curve of the chondrite is relatively flat, with obvious positive Ce (δCe = 0.10–16.72) and negative Eu (δEu = 0.48–0.82) anomalies (Fig. 9).

Chondrite-normalized REE patterns in the HLF transition zone is left-inclining (HREE/LREE enrichment), different from those of the UC, UAl and ComB horizons (Fig. 9). LREE is more enriched in UC, while HREE is more enriched in UC transition zone to HLF (Fig. 10), indicating stronger fractionation of LREE and HREE in the profile with distance.

4.6. Distribution patterns of critical metals (Li-Ga-Zr-Sc-REE)

Lithium content is high in the bauxitic clay OBC and UBC (Table 1; Fig. 10), above the minimum industrial grade of 260 ppm (Jin et al., 2019). Among the bauxite layers, only ComB is Li-rich, with EC = 85.56. This layer is adjacent to the underlying rock layer (UAl: 46.4 wt% Al_2O_3 and 1.83 A/S; Table 1; Fig. 10), which is just above the division boundary between bauxite and bauxitic clay, and its characteristics resemble more the latter. Therefore, we group this Li-rich layer into bauxitic clay in the following discussion. The EC of Li is 47.03–63.71 for OBC and 48.25–60.14 for UBC, which is at least an order of magnitude above that of the bauxite layer (0.39–5.96, except for ComB; Fig. 7). This confirms that Li is mainly enriched in the bauxitic clay at the top and bottom parts of the bauxite (r = 0.83; Fig. 11). The Kernel density curves show that the Li distribution is highly similar to that of Al_2O_3 and SiO_2, as featured by the presence of two peaks (Fig. 11). The smoothed fit curve shows that the Li content increases significantly with SiO_2, and then plateau at ~25 wt% SiO_2. The Li content first increases slightly (before Al_2O_3 <40 wt%), and then gradually decreases with increasing

Table 1
Compositions of major and trace elements. QF-Qixia Fm, LF-Liangshan Fm, OC-Overlying clay rock, OAl-Overlying aluminite, PisB-Bean-like bauxite, ClsB-Clastic bauxite, EseB-Earthy-semi-earthy bauxite, ComB-Compact bauxite, UAl- Underlying aluminite, UC-Underlying claystone, HlF-Huanglong Fm.

Elements	ZK805-2	ZK805-3	ZK805-4	ZK805-5	ZK805-6	ZK805-7	ZK805-8	ZK805-9	ZK805-10	ZK805-11	ZK805-12	ZK805-13	ZK805-14	ZK805-15	ZK805-16	ZK805-17	ZK805-18	ZK805-19	ZK805-20	ZK805-21	ZK805-22	ZK805-23	ZK4A01-1
Lithology	LF	OAl	OAl	OAl	PisB	PisB	PisB	ClsB	ClsB	EseB	EseB	EseB	EseB	EseB	ComB	UAl	UAl	UAl	UC	UC	UC	HlF	QF
Major elemnts(.wt%)																							
Al_2O_3	33.79	38.97	41.01	37.14	55.93	53.27	64.21	67.33	64.39	71.78	74.10	68.20	68.06	74.48	46.44	40.01	44.02	42.17	37.46	35.82	36.61	4.89	1.01
SiO_2	38.14	36.94	28.86	26.85	10.69	16.67	6.80	6.93	9.86	4.20	4.41	6.02	7.56	3.86	25.28	36.42	33.18	37.12	42.01	39.94	40.44	4.99	12.21
Fe_2O_3	6.10	2.70	5.63	10.36	11.47	4.38	5.94	2.55	2.62	1.66	1.03	2.84	2.55	1.58	5.74	4.72	4.64	2.12	2.62	5.11	4.40	5.80	2.24
MgO	2.41	3.65	5.10	5.57	3.02	4.83	2.05	2.28	3.31	1.40	1.45	1.88	2.58	1.30	5.42	2.41	2.57	1.89	1.78	2.11	2.66	1.49	10.37
CaO	0.37	0.40	0.23	0.21	0.080	0.18	0.090	0.14	0.10	0.090	0.060	0.10	0.10	0.080	0.20	0.14	0.13	0.15	0.20	0.20	0.21	44.74	38.12
Na_2O	0.060	0.060	0.060	0.060	0.040	0.06	0.050	0.050	0.050	0.050	0.050	0.050	0.060	0.050	0.050	0.050	0.060	0.050	0.16	0.060	0.080	0.070	0.080
K_2O	3.32	1.41	0.58	0.36	0.15	0.23	0.040	0.040	0.020	bdl	bdl	0.020	0.030	bdl	0.65	0.10	0.12	0.22	0.21	0.22	0.25	0.13	0.20
MnO	0.024	0.018	0.017	0.012	0.012	0.015	0.011	0.015	0.014	0.008	0.010	0.011	0.012	0.010	0.026	0.024	0.024	0.013	0.02	0.018	0.019	0.20	1.43
P_2O_5	0.024	0.043	0.044	0.040	0.035	0.046	0.052	0.083	0.059	0.078	0.064	0.068	0.071	0.10	0.068	0.14	0.065	0.074	0.090	0.056	0.052	0.059	0.042
TiO_2	2.03	2.47	2.03	1.80	3.21	3.15	3.37	3.12	3.03	3.91	3.66	3.34	3.18	2.91	3.25	2.06	2.07	1.90	1.74	1.66	1.70	0.28	0.053
LOI	13.44	12.75	15.23	16.39	15.13	17.98	17.15	16.75	15.37	16.16	14.87	16.49	15.30	14.97	12.18	12.99	12.92	13.31	13.43	13.97	13.11	36.12	33.13
Total	99.71	99.42	98.79	98.79	99.76	100.81	99.76	99.29	98.82	99.34	99.71	99.02	99.50	99.35	99.30	99.05	99.79	99.01	99.71	99.16	99.53	98.75	98.88
A/S	0.89	1.05	1.42	1.38	5.23	3.20	9.44	9.72	6.53	17.09	16.80	11.33	9.00	19.30	1.84	1.10	1.33	1.14	0.89	0.90	0.91	0.98	0.083
Rare elements(ppm)																							
Li	556	725	822	1018	204	77.8	12.5	8.11	17.6	5.17	6.45	10.3	10.6	4.79	1540	879	1002	1440	918	955	996	37.2	6.15
Be	6.27	4.91	4.84	3.4	4.49	4.11	4.25	3.86	3.59	3.64	3.64	3.45	3.43	3.34	2.77	3.78	3.69	3.35	4.43	4.07	4.85	0.692	0.304
V	395	284	308	228	322	259	264	327	326	774	343	525	407	337	304	212	231	288	223	270	268	32.3	13.3
Cr	332	235	242	180	273	276	276	258	201	188	184	233	201	152	230	122	130	154	138	170	173	26.2	20.3
Co	3.38	2.48	2.55	2.76	5.60	11.1	13.5	9.20	14.5	6.04	3.18	14.9	7.39	5.99	6.46	12.5	11.5	14.4	16.5	33.8	21.5	20.1	3.08
Ni	12.0	3.81	3.04	3.77	7.82	6.19	8.45	6.78	12.2	7.38	7.41	20.8	17.3	12.7	36.3	80.7	74.2	93.3	110	129	117	67.2	21.7
Cu	11.9	14.7	12.3	24.6	26.4	44.7	25.0	22.5	25.1	24.3	21.6	24.2	21.4	18.7	21.4	17.1	16.8	148	28.8	24.3	13.3	781	3.04
Zn	32.2	41.8	43.8	48.5	65.2	58.7	49.5	50.6	56.9	53.7	51.5	50.4	53.2	43.0	83.3	49.0	51.9	45.6	45.3	48.1	57.1	40.5	13.0
Ga	44.6	45.8	56.6	41.1	57.4	56.7	42.6	38.6	34.8	35.1	33.7	32.0	31.7	32.9	56.0	27.2	34.4	31.8	23.7	27.8	31.9	8.16	2.30
Ge	0.499	0.471	0.619	0.863	1.95	2.06	2.64	2.72	1.77	2.64	2.02	1.78	1.86	2.09	1.23	1.26	1.47	0.992	1.07	1.01	0.995	0.786	0.152
As	44.2	13.2	33.7	31.7	12.6	33.0	24.1	20.3	19.4	7.34	2.05	59.7	11.3	10.6	6.04	12.9	9.88	7.00	6.01	24.7	5.26	2.46	4.29
Rb	81.0	33.6	16.1	10.2	6.72	4.31	1.27	1.20	0.903	0.322	0.336	0.677	0.906	0.359	15.1	4.21	4.66	7.52	6.31	7.35	8.24	4.87	7.28
Sr	240	200	143	110	67.3	50.7	24.2	21.6	30.0	23.5	20.1	33.7	57.3	87.2	258	514	162	167	207	141	138	215	815
Zr	600	749	660	616	1027	986	1049	1047	975	1121	1196	975	748	587	733	445	422	400	414	385	429	53.4	10.5
Nb	40.8	57.6	44.8	40.7	76.3	73.7	73.3	73.1	72.0	89.6	85.3	79.0	74.2	66.4	78.0	45.8	46.2	41.7	37.7	35.4	37.4	5.45	1.22
Mo	2.07	1.67	1.69	4.17	4.29	4.55	1.87	7.98	5.49	4.54	4.82	10.8	4.04	5.27	2.43	0.554	0.596	0.599	1.08	1.57	1.07	0.435	4.53
Ag	1.49	1.80	1.61	1.44	2.41	2.40	2.32	2.42	2.32	2.74	2.54	2.44	2.34	2.03	2.44	1.62	1.56	1.59	1.29	1.32	1.30	0.447	0.226
Cd	0.648	0.445	0.864	0.531	0.619	1.41	0.629	0.650	0.560	0.575	0.511	0.56	0.506	0.470	0.527	0.364	0.337	0.303	0.278	0.321	0.282	2.94	1.96
In	0.211	0.181	0.213	0.218	0.296	0.314	0.261	0.260	0.296	0.194	0.197	0.218	0.252	0.167	0.397	0.184	0.179	0.220	0.183	0.183	0.179	0.031	0.008
Sn	9.40	10.9	13.2	12.0	11.8	17.1	15.6	14.8	14.8	17.7	17.3	15.0	15.9	15.1	17.3	11.6	10.4	9.59	9.09	8.94	9.17	0.983	0.433
Sb	2.50	1.27	3.27	2.14	1.45	2.99	2.30	1.29	1.32	0.985	0.69	1.80	1.41	0.938	0.959	1.43	1.21	0.841	0.742	2.33	0.548	0.156	0.249
Cs	17.8	8.46	6.01	3.71	0.665	0.192	0.084	0.085	0.111	0.039	0.042	0.081	0.097	0.054	1.08	2.00	2.16	2.45	1.85	2.15	2.50	0.57	0.371
Ba	258	145	196	80.2	28.6	25.5	8.72	8.09	19.1	6.80	6.13	7.66	8.66	6.79	55.9	37.3	35.8	37.7	26.6	27.5	32.0	20.0	15.4
Hf	15.4	18.8	17.0	15.4	25.8	25.0	27.1	26.9	24.6	28.6	30.2	24.4	19.0	15.0	18.9	12.3	11.7	10.9	11.5	10.7	11.5	2.11	0.287
Ta	3.04	4.13	3.34	3.03	5.09	5.02	4.93	4.99	4.94	6.03	5.74	5.27	5.12	4.64	5.56	3.35	3.37	3.07	2.72	2.59	2.73	0.456	0.158
W	4.20	4.82	4.04	3.55	5.59	5.68	5.42	6.11	6.32	7.05	6.58	6.2	5.18	4.95	5.63	4.31	4.59	6.71	3.28	3.12	3.14	0.750	0.203
Tl	0.503	0.188	0.389	0.592	0.520	0.501	0.318	0.224	0.137	0.108	0.030	1.46	0.235	0.033	0.175	0.095	0.072	0.073	0.059	0.172	0.048	0.04	0.079
Pb	62.2	23.6	90.8	51.0	27.9	136	54.6	38.1	18.5	19.4	8.28	19.5	17.4	26.3	20.7	50.6	25.4	33.7	13.9	119	8.81	21.3	44.5
Bi	1.08	0.739	0.834	0.776	0.701	0.707	1.15	0.432	0.633	1.75	0.541	1.13	0.863	0.681	1.14	0.564	0.467	0.694	0.525	0.742	0.448	0.244	0.039
Th	61.8	44.1	45.3	43.7	57.6	55.5	64.4	38.5	41.4	29.7	21.2	30.1	38.1	22.0	48.1	32.3	33	41.4	34.3	35.9	34.1	4.51	1.17
U	5.77	6.31	5.68	6.01	9.01	9.42	12.6	12.4	15.0	18.9	13.4	13.0	12.1	13.6	11.6	7.15	6.17	6.90	4.61	4.42	4.81	1.51	4.45
Sc	11.0	10.6	14.4	17.2	14.5	15.8	11.3	7.43	10.8	7.87	8.51	10.3	15.1	6.62	60.6	20.2	19.0	15.0	21.3	28.1	34.4	4.76	1.29
La	2.20	2.65	1.54	0.708	2.00	1.72	0.892	0.845	1.46	1.55	1.12	2.35	5.79	17.7	25.7	45.5	24.3	35.7	53.4	37.5	37.9	15.3	4.70

(*continued on next page*)

Table 1 (*continued*)

Elements	ZK805-2	ZK805-3	ZK805-4	ZK805-5	ZK805-6	ZK805-7	ZK805-8	ZK805-9	ZK805-10	ZK805-11	ZK805-12	ZK805-13	ZK805-14	ZK805-15	ZK805-16	ZK805-17	ZK805-18	ZK805-19	ZK805-20	ZK805-21	ZK805-22	ZK805-23	ZK4A01-1
Lithology	LF	OAl	OAl	OAl	PisB	PisB	PisB	ClsB	ClsB	EseB	EseB	EseB	EseB	EseB	ComB	UAl	UAl	UAl	UC	UC	UC	HlF	QF
Major elemnts(.wt%)																							
Ce	5.48	6.64	4.70	2.32	6.29	7.44	3.83	3.23	9.41	10.3	8.54	19.6	46.0	113	189	507	187	246	411	435	510	23.3	7.35
Pr	0.561	0.639	0.404	0.187	0.443	0.460	0.264	0.190	0.281	0.303	0.242	0.496	1.06	2.94	4.08	7.87	3.9	5.24	7.95	8.37	10.2	4.82	1.02
Nd	2.53	2.81	1.78	0.889	1.88	2.03	1.30	0.869	1.15	1.28	0.98	1.96	3.73	10.4	13.9	24.8	12.5	16.3	24.8	31.7	40.9	26.1	4.33
Sm	1.16	1.06	0.876	0.582	0.898	0.891	0.879	0.571	0.589	0.656	0.531	0.833	1.15	2.07	3.28	4.16	2.07	2.79	4.46	7.41	10.2	17.1	1.03
Eu	0.394	0.396	0.369	0.253	0.341	0.319	0.336	0.218	0.224	0.240	0.186	0.284	0.365	0.423	0.754	0.761	0.396	0.483	0.679	1.19	1.78	6.67	0.258
Gd	2.34	2.21	2.21	1.61	2.02	1.90	2.15	1.46	1.54	1.69	1.40	1.99	2.03	1.72	3.70	3.90	2.38	2.87	4.18	6.69	9.07	41.5	1.06
Tb	0.535	0.485	0.509	0.394	0.476	0.470	0.483	0.328	0.363	0.389	0.335	0.437	0.442	0.299	0.760	0.550	0.479	0.528	0.637	0.965	1.23	7.24	0.160
Dy	4.55	3.93	4.19	3.35	3.97	3.98	3.97	2.68	3.10	3.24	2.88	3.56	3.55	2.16	6.26	3.55	3.79	4.08	4.25	6.02	7.08	50.7	0.969
Ho	1.07	0.913	0.953	0.763	0.916	0.947	0.888	0.600	0.719	0.732	0.673	0.786	0.812	0.489	1.51	0.798	0.899	0.947	0.943	1.29	1.41	10.0	0.191
Er	3.15	2.69	2.81	2.30	2.78	2.87	2.56	1.74	2.13	2.10	1.95	2.32	2.38	1.46	4.76	2.51	2.83	3.00	3.00	4.03	4.31	21.8	0.511
Tm	0.516	0.446	0.461	0.389	0.472	0.484	0.42	0.287	0.353	0.34	0.316	0.368	0.391	0.238	0.821	0.422	0.486	0.509	0.517	0.695	0.738	2.41	0.071
Yb	3.42	3.15	3.24	2.78	3.46	3.53	2.96	2.09	2.54	2.43	2.24	2.62	2.79	1.67	5.91	3.02	3.36	3.48	3.58	4.93	5.19	11.4	0.429
Lu	0.514	0.481	0.502	0.427	0.545	0.543	0.444	0.308	0.383	0.355	0.324	0.384	0.418	0.246	0.907	0.468	0.524	0.518	0.551	0.764	0.81	1.44	0.062
Y	32.7	27.9	30	23.6	27.8	27.9	26.8	17.9	20.7	21.5	20.4	23.3	22.5	13.7	40.5	20.1	21.7	21.5	21.3	29.0	31.9	501	7.03
REE	61.1	56.4	54.5	40.6	54.3	55.5	48.2	33.3	44.9	47.1	42.1	61.3	93.4	168	302	625	266	344	542	576	673	741	29.2

Elements	ZK4A01-2	ZK4A01-3	ZK4A01-4	ZK4A01-5	ZK4A01-6	ZK4A01-7	ZK4A01-8	ZK4A01-9	ZK4A01-10	ZK4A01-11	ZK4A01-12	ZK4A01-13	ZK4A01-14	ZK4A01-15	ZK4A01-16	ZK4A01-17	ZK4A01-18	ZK4A01-19	ZK4A01-20	ZK4A01-21	ZK4A01-22	ZK4A01-23	ZK4A01-24
Lithology	LF	OC	OC	OAl	OAl	PisB	PisB	PisB	PisB	PisB	PisB	ClsB	ClsB	ClsB	ClsB	ClsB	ClsB	UAl	UAl	UC	UC	UC	HlF
Major elemnts(.wt%)																							
Al_2O_3	23.26	35.34	37.12	43.69	44.73	55.59	62.70	49.75	66.46	66.95	67.67	60.91	55.79	55.53	54.74	55.86	56.90	36.50	35.01	34.45	34.27	29.82	4.22
SiO_2	40.16	37.12	38.84	29.81	29.08	8.94	10.46	4.51	4.55	4.62	5.39	8.16	10.16	10.23	10.56	9.87	9.90	34.65	38.34	37.67	38.72	37.28	4.53
Fe_2O_3	9.88	5.54	3.00	3.56	3.62	12.08	4.52	17.99	6.39	6.19	5.41	11.46	15.14	15.67	16.52	15.59	14.29	9.17	8.37	8.46	9.14	14.34	5.91
MgO	2.89	4.04	4.58	5.94	5.61	2.67	3.16	1.33	1.27	1.36	1.57	2.15	2.60	2.60	2.67	2.51	2.55	4.37	3.45	4.08	3.26	4.44	1.46
CaO	0.40	0.30	0.32	0.21	0.29	0.090	0.10	0.100	0.080	0.090	0.090	0.070	0.060	0.060	0.060	0.080	0.060	0.19	0.21	0.23	0.23	0.31	45.75
Na_2O	0.080	0.080	0.070	0.070	0.070	0.080	0.070	0.050	0.070	0.070	0.070	0.070	0.080	0.080	0.070	0.070	0.070	0.070	0.070	0.10	0.070	0.080	0.080
K_2O	5.71	1.62	0.96	0.29	0.23	0.060	0.040	0.010	0.010	bdl	0.010	bdl	0.010	bdl	0.010	0.010	0.020	0.34	0.44	0.57	0.87	3.97	0.16
MnO	0.040	0.018	0.017	0.017	0.013	0.015	0.013	0.015	0.014	0.018	0.018	bdl	bdl	bdl	bdl	bdl	bdl	bdl	bdl	bdl	bdl	0.04	0.21
P_2O_5	0.14	0.024	0.054	0.047	0.13	0.065	0.072	0.040	0.082	0.11	0.10	0.094	0.10	0.070	0.053	0.052	0.060	0.057	0.058	0.074	0.071	0.12	0.084
TiO_2	1.07	1.89	1.83	2.18	2.43	2.78	3.74	2.30	3.23	2.74	3.02	3.02	2.57	2.57	2.18	2.57	2.76	1.76	1.69	1.51	1.45	1.60	0.18
LOI	15.64	13.29	12.70	13.19	13.21	17.17	14.35	22.19	16.87	16.88	15.67	13.17	12.27	12.24	11.68	12.17	12.04	11.91	11.94	11.99	11.32	7.92	36.88
Total	99.28	99.26	99.48	99.00	99.42	99.54	99.22	98.28	99.02	99.03	99.03	99.11	98.77	99.04	98.53	98.79	98.66	99.02	99.58	99.14	99.40	99.91	99.47
A/S	0.58	0.95	0.96	1.47	1.54	6.22	5.99	11.03	14.61	14.49	12.55	7.46	5.49	5.43	5.18	5.66	5.75	1.05	0.91	0.91	0.89	0.80	0.93
Rare elements(ppm)																							
Li	72.5	861	1035	1048	1255	38.5	49.5	23.5	14.9	15.8	14.0	71.2	120	90.7	143	118	116	982	768	499	510	205	23.5
Be	7.20	6.46	5.22	5.46	6.79	5.35	5.77	3.43	4.39	4.42	4.50	4.49	4.46	4.46	4.65	4.94	5.46	5.86	7.12	5.44	6.07	6.35	0.584
V	238	299	241	206	167	183	495	399	428	553	621	263	239	229	226	227	241	217	173	161	157	183	40.0
Cr	270	255	233	243	198	217	269	217	246	203	232	185	159	148	117	129	146	118	103	106	107	161	23.1
Co	18.1	13.3	11.6	18.8	18.9	40.2	36.8	68.3	25.8	31.0	22.1	15.7	17.6	15.8	19.8	21.1	20.1	62.8	39.9	57.2	48.2	69.0	25.0
Ni	33.5	5.06	3.56	6.65	7.55	16.1	13.8	16.4	14.2	22.5	19.7	29.7	25.6	25.5	28.9	29.7	45.6	227	199	238	222	220	55.7
Cu	22.2	13.2	12.4	15.6	16.7	45.8	40.8	40.2	21.8	58.4	17.9	25.9	27.2	59.1	93.2	26.4	16.0	60.8	66.7	25.2	30.5	155	76.8
Zn	48.3	45.3	40.8	76.3	82.0	58.0	105	40.8	51.3	56.1	55.1	76.8	106	73.6	75.8	77.5	78.0	113	116	131	116	166	49.8
Ga	49.8	47.2	43.2	47.4	41.2	44.5	42.1	44.7	47.1	41.7	39.4	37.1	43.2	39.7	44.7	43.9	50.5	33.5	27.4	33.6	31.8	39.8	7.04
Ge	0.79	0.552	0.473	0.860	1.06	2.37	2.59	1.90	2.55	2.92	2.72	3.74	3.87	3.74	4.07	4.72	5.38	1.07	0.911	0.953	0.918	2.64	0.443
As	57.4	16.6	9.98	9.59	10.7	50.4	28.2	94.3	59.5	92.4	69.4	14.4	9.07	11.2	5.69	9.51	11.4	54.6	4.24	2.21	1.65	5.99	1.26
Rb	224	35.9	22.0	8.96	7.29	1.82	1.420	0.454	0.255	0.269	0.291	0.206	0.203	0.173	0.249	0.264	0.435	12.5	15.4	18.0	26.3	146	6.88
Sr	191	164	108	138	137	39.2	46.4	37.6	62.3	125	72.4	233	333	182	85.5	85.6	99.2	155	155	234	208	423	194
Zr	230	540	592	722	840	863	1299	699	976	736	853	664	560	510	682	986	882	580	489	371	380	388	49.2

(*continued on next page*)

Table 1 (*continued*)

Elements	ZK805-2	ZK805-3	ZK805-4	ZK805-5	ZK805-6	ZK805-7	ZK805-8	ZK805-9	ZK805-10	ZK805-11	ZK805-12	ZK805-13	ZK805-14	ZK805-15	ZK805-16	ZK805-17	ZK805-18	ZK805-19	ZK805-20	ZK805-21	ZK805-22	ZK805-23	ZK4A01-1
Lithology	LF	OAl	OAl	OAl	PisB	PisB	PisB	ClsB	ClsB	EseB	EseB	EseB	EseB	EseB	ComB	UAl	UAl	UAl	UC	UC	UC	HlF	QF
Major elemnts(.wt%)																							
Nb	23.4	40.3	41.5	46.1	61.3	62.4	92.4	50.1	77.5	59.3	71.1	75.4	63.7	53.7	49.2	63.4	71.3	41.8	40.1	34.6	34.1	35.2	3.64
Mo	13.2	2.62	1.4	3.46	3.06	3.55	4.21	3.12	2.97	3.62	3.66	0.887	0.607	0.809	1.10	0.910	1.10	0.936	0.642	0.696	0.564	0.444	0.362
Ag	0.795	1.35	1.16	1.34	1.51	1.95	2.27	1.82	2.06	1.85	1.92	1.98	1.70	1.55	1.51	1.8	1.91	1.29	1.24	1.11	1.06	1.13	0.186
Cd	0.439	0.444	0.369	0.602	0.524	0.841	1.03	1.29	0.945	3.40	1.31	2.14	4.53	0.412	0.39	0.378	0.482	0.301	0.278	0.265	0.253	0.285	2.61
In	0.116	0.18	0.189	0.186	0.205	0.190	0.226	0.213	0.188	0.213	0.196	0.203	0.241	0.246	0.236	0.202	0.216	0.200	0.164	0.174	0.163	0.156	0.03
Sn	5.26	9.90	10.9	11.5	11.8	14.4	16.8	12.7	14.9	14.1	15.9	15.3	13.7	13.3	11.1	11.8	15.2	9.82	9.07	8.72	8.33	7.79	1.03
Sb	3.49	1.64	1.20	1.41	1.07	2.90	2.22	6.50	5.08	2.43	2.13	0.609	0.437	0.505	0.484	0.554	0.686	0.592	0.463	0.411	0.381	0.548	0.063
Cs	16.8	8.10	6.97	4.18	2.91	0.265	0.248	0.061	0.051	0.071	0.087	0.078	0.072	0.064	0.074	0.057	0.125	3.51	3.38	4.00	3.92	9.75	0.526
Ba	264	103	69.4	36.3	37.7	17.8	8.86	5.83	6.29	6.56	5.67	7.30	6.17	5.44	5.96	7.12	7.87	205	39.3	47.5	58.1	165	1642
Hf	6.42	14.1	15.6	19.7	22.1	22.9	33.9	18.7	26.5	17.9	20.5	16.4	13.9	12.6	16.2	23.5	21.0	14.6	12.7	10.3	10.3	11.3	2.24
Ta	1.62	2.96	3.10	3.43	4.12	4.25	6.34	3.87	5.26	4.11	4.62	4.99	4.25	4.02	3.63	4.24	4.68	3.01	2.90	2.60	2.55	2.68	0.431
W	2.30	3.64	3.73	6.14	6.75	6.05	8.97	4.71	6.58	4.94	5.51	5.60	4.72	4.58	4.43	5.25	5.90	4.11	4.07	3.40	3.42	3.67	0.598
Tl	1.53	0.518	0.398	0.437	0.439	0.971	0.29	1.46	0.611	1.29	0.668	0.176	0.073	0.141	0.044	0.030	0.034	0.105	0.112	0.114	0.157	0.707	0.035
Pb	69.4	25.1	14.4	185	105	110	39.2	128	40.4	99.3	14.5	6.93	4.48	4.42	4.62	6.18	6.02	12.4	6.51	10.7	5.84	12.5	10.7
Bi	0.647	0.662	0.544	0.513	0.55	0.579	0.459	0.823	0.983	1.87	1.07	0.450	0.254	0.125	0.203	0.411	0.368	0.852	0.651	0.652	0.415	0.559	0.283
Th	24.5	49.7	52.3	60.0	53.4	42.0	50.1	38.9	47.4	35.7	33.9	36.0	34.1	34.6	26.5	29.8	40.8	35.8	33.2	34.6	33.2	32.4	3.87
U	18.3	6.35	5.82	6.54	9.10	9.15	13.2	8.36	12.3	10.3	11.9	10.1	8.08	6.72	5.46	6.70	7.59	4.46	3.87	3.92	3.69	4.26	1.36
Sc	16.9	14.8	13.1	11.9	12.9	9.18	12.3	14.4	14.4	13.6	12.4	18.0	20.5	20.2	21.2	18.1	21.4	30.8	26.0	26.2	24.0	24.8	4.815
La	60.7	2.62	3.10	3.16	2.90	2.95	4.38	2.43	3.08	3.63	2.37	9.95	11.1	11.4	12.8	14.5	19.9	29.0	45.4	85.5	104	1230	36.7
Ce	111	11.7	11.0	19.9	18.0	14.9	23.8	21.2	41.6	92.0	46.6	205	294	235	426	360	186	150	224	222	226	206	24.3
Pr	12.3	0.644	0.660	0.706	0.873	0.639	0.901	0.546	0.702	1.09	0.618	2.11	2.42	1.92	2.42	2.55	2.78	4.26	9.41	12.7	14.7	176	8.90
Nd	43.5	2.90	2.80	3.01	4.08	2.70	3.63	2.29	3.22	5.09	2.98	8.20	9.19	6.49	9.10	9.35	8.32	12.3	33.3	37.0	47.9	693	46.3
Sm	5.71	1.10	1.10	1.27	2.01	1.28	1.65	1.05	1.32	1.69	1.16	2.26	2.41	1.56	2.88	2.70	1.75	2.85	8.39	7.15	11.0	123	21.0
Eu	1.02	0.378	0.379	0.444	0.67	0.43	0.526	0.337	0.406	0.43	0.351	0.614	0.592	0.416	0.618	0.575	0.387	0.559	1.53	1.16	1.89	24.0	7.26
Gd	4.81	2.32	2.45	3.00	4.14	3.06	3.80	2.35	2.73	2.47	2.22	3.23	3.53	2.96	4.46	4.07	2.84	3.74	7.54	6.47	9.29	104	49.7
Tb	0.719	0.529	0.556	0.694	0.861	0.761	0.939	0.589	0.662	0.538	0.526	0.654	0.674	0.644	0.684	0.685	0.666	0.912	1.42	1.36	1.78	14.8	10.2
Dy	4.10	4.24	4.38	5.41	6.39	6.24	7.85	4.91	5.74	4.38	4.39	5.45	5.68	5.73	5.28	5.57	6.14	7.92	10.1	10.1	12.2	79.5	77.3
Ho	0.853	0.926	0.954	1.16	1.33	1.34	1.70	1.08	1.26	0.973	0.969	1.29	1.35	1.39	1.25	1.37	1.55	1.90	2.19	2.20	2.51	14.7	17.0
Er	2.71	2.75	2.75	3.30	3.63	3.83	4.79	3.04	3.60	2.73	2.72	3.79	4.12	4.27	3.95	4.39	5.17	6.35	7.18	7.14	7.91	38.4	41.6
Tm	0.44	0.45	0.451	0.514	0.569	0.584	0.754	0.484	0.562	0.423	0.422	0.615	0.68	0.714	0.683	0.777	0.934	1.25	1.37	1.36	1.49	5.06	4.81
Yb	3.11	3.13	3.11	3.49	3.80	3.98	5.08	3.15	3.73	2.76	2.79	4.09	4.55	4.82	4.80	5.49	6.64	9.50	10.7	10.3	11.3	29.4	22.4
Lu	0.499	0.47	0.473	0.533	0.564	0.591	0.758	0.47	0.536	0.404	0.408	0.614	0.682	0.733	0.745	0.855	1.05	1.52	1.74	1.66	1.80	4.29	3.07
Y	23.5	27.8	28.8	33.4	36.0	36.6	44.8	28.3	33.1	26.2	26.5	30.5	31.7	30.9	26.9	28.9	31.4	37.1	40.9	40.2	47.1	339	810
REE	275	62.0	62.9	80.0	85.8	79.9	105	72.2	102	145	95.0	278	373	309	503	442	275	269	405	447	501	3082	1181

bdl = below detection limit.

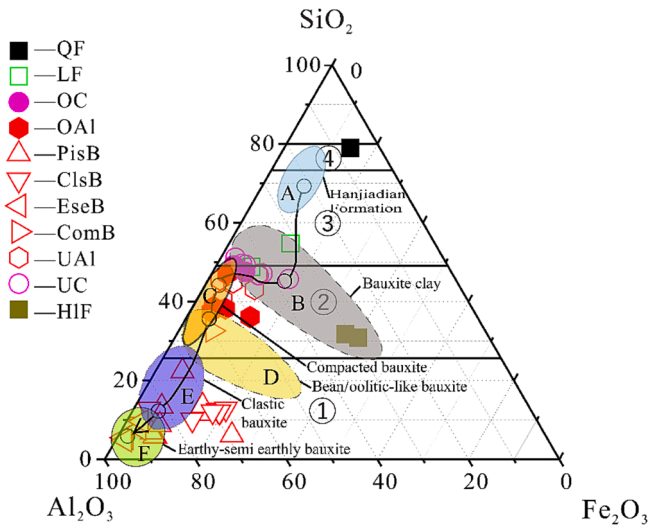

Fig. 6. Ternary SiO_2-Al_2O_3-Fe_2O_3 plot for the Danping ore-host samples (Schellmann, 1982). The shaded area denotes the bauxite range of the Wuchan-Zheng'an-Daozhen (WZD; (Huang et al., 2014)). A, B, C, D, E, and F are representative samples from the exploration trench of Xinmin bauxite in WZD. The scatter plot is a sample of the Danping bauxite ore host, with the sample number shown in Table 1. ①-Strong lateritization, ②-Moderate lateritization, ③-Weak lateritization, ④-Kaolinitization.

Al_2O_3. This suggests that with the continuous clayification, desilicification, alumina enrichment, and Li enrichment in clay minerals, substantial amount of Li was adsorbed by clay minerals or enriched with Al-rich mineral (such as chlorite), which may explain the positive Al vs. Li correlation in the early-stage bauxite ore (Fig. 11). Thus, we proposed that Li was mainly enriched in the clay mineralization stage.

Gallium occurs in all layers of the ore host (Table 1; Fig. 10), with concentration above the minimum industrial grade (20 ppm; MRIRMEC, 2010). It is more enriched in the middle and upper parts of the profile, consistent with the peaks of the Ga kernel density curve (Fig. 11). The EC (Ga) is 2.20–3.73 for the bauxite, 2.95–3.16 for OBC, and 1.84–2.33 for UBC (Fig. 7). The Ga vs. Al_2O_3 smooth-fit curve (Fig. 11) shows that the Ga content increases first and then decreases with increasing Al_2O_3 content, reaching a peak at 50–60 wt% Al_2O_3. This indicates that Ga is enriched in all ore/rock layers, which warrant further research and exploration.

Zirconium is more abundant in the bauxite horizon (Table 1; Fig. 10), above the minimum industrial grade (296 ppm) for coastal sand-type resource (Huang et al., 2014). The EC (Zr) is 3.42–5.03 for the bauxite, 2.78–3.84 for OBC, and 1.87–2.62 for UBC (Fig. 7). Both linear and smoothed fit curves show strongly positive Al_2O_3 vs. TiO_2 correlation (r = 0.74, 0.88), indicating high degree of coupling for their fractionation enrichment (Fig. 11).

Scandium is slightly enriched in some bauxite and OBC, and more enriched in/around the UBC, with EC = 1.12–3.78 (Table 1; Figs. 7 and 10). Scandium enrichment is correlated positively with SiO_2 (r = 0.44; Fig. 11), implying that the Sc is associated with Si-rich minerals.

The REE distribution indicates that REE are mainly enriched in bauxitic clay or claystone in the lower part of the profile, above the minimum industrial grade of 500 ppm (MRIRMEC, 2010). In the ore host, LREE and HREE are enriched in different rock types (Table 1; Fig. 10): LREE are enriched in the UBC (EC = 1.94–5.48; Fig. 7, especially UC), and locally in the bauxite layers adjacent to the basement rocks, e.g., ComB in ZK805 (EC = 1.82) and ClsB in ZK4A01 (EC = 2.30); while HREE are more enriched in the UBC (EC = 1.34–4.45) and its adjacent HLF tuff transition zone (EC = 17.04–27.26). The positive correlation between LREE and HREE (Fig. 11) indicates that REE distributions are very similar. Meanwhile, Table 1 and Figs. 9 and 10 can also indicate the differentiation between LREE and HREE, especially the significant enrichment of Y in the UC (E = 10.46–16.15) and HLF transition zones (EC = 20.88–33.75).

5. Discussion

5.1. Distribution mechanism of critical metals (Li-Ga-Zr-Sc-REE)

Lithium is significantly enriched during moderate lateritizaton. Analysis show that the Li content is the highest in the kaolinitic bauxite zone, indicating that clay minerals have played a key role in Li enrichment, as also supported by the positive Li vs. SiO_2 correlation (r = 0.83; Figs. 6, 12 and 13).

Moreover, the positive Li vs. Al_2O_3 correlations (also mainly from clay minerals in the OBC and UBC) suggest the Li affinity with aluminosilicates (Fig. 11; (Sun et al., 2016; Wang et al., 2013a)). Therefore, clay minerals (illite, kaolinite, and smectite) and chlorite are the most probable Li host. The higher Li content in the OBC and UBC than the bauxite layer is probably caused by that the former two contain more clay minerals than the latter.

As shown in Figs. 6 and 13, Ga is gradually enriched during lateritization, and is thus much higher in the bauxite and kaolinite-bauxite zones than in the other zones (Fig. 13). Zirconium is significantly

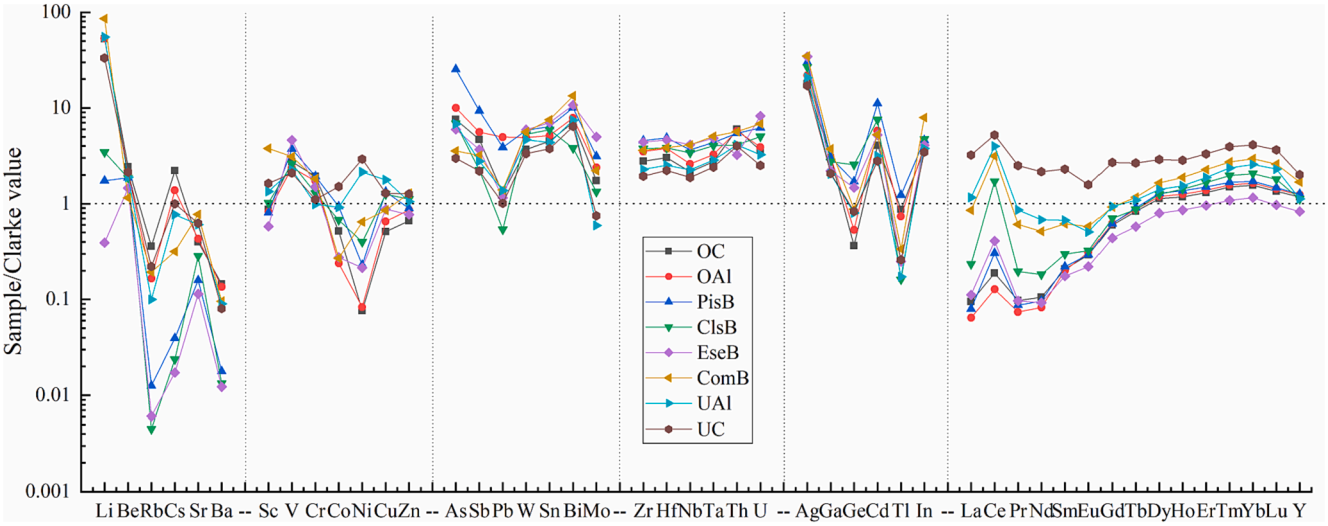

Fig. 7. Clarke value-normalized plots for Li, Ga, Zr, Sc, and REE (geometric mean value) from the Danping bauxite profile (Wedepohl, 1995).

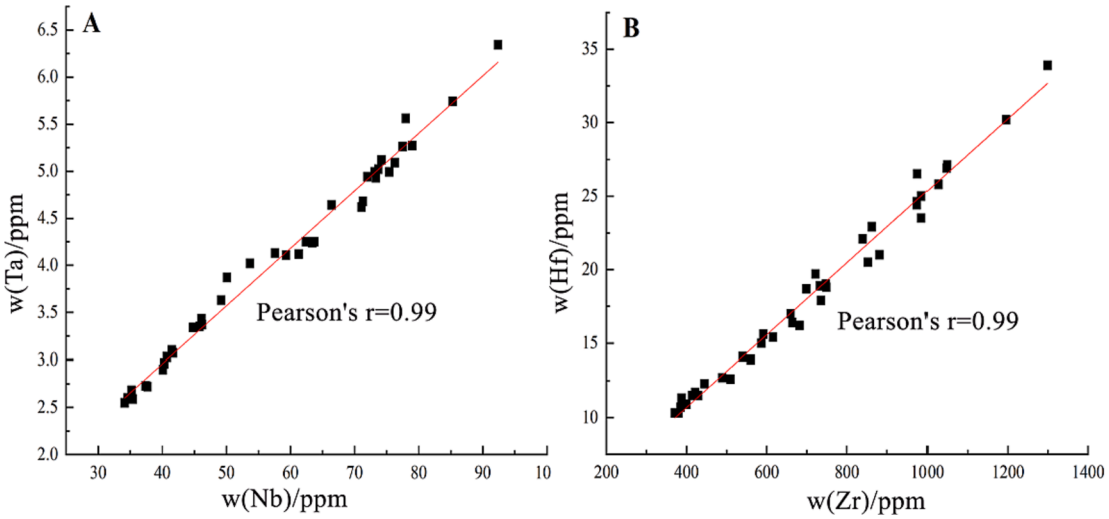

Fig. 8. Diagrams of Nb vs. Ta and Zr vs. Hf for the Danping bauxite ore-host series.

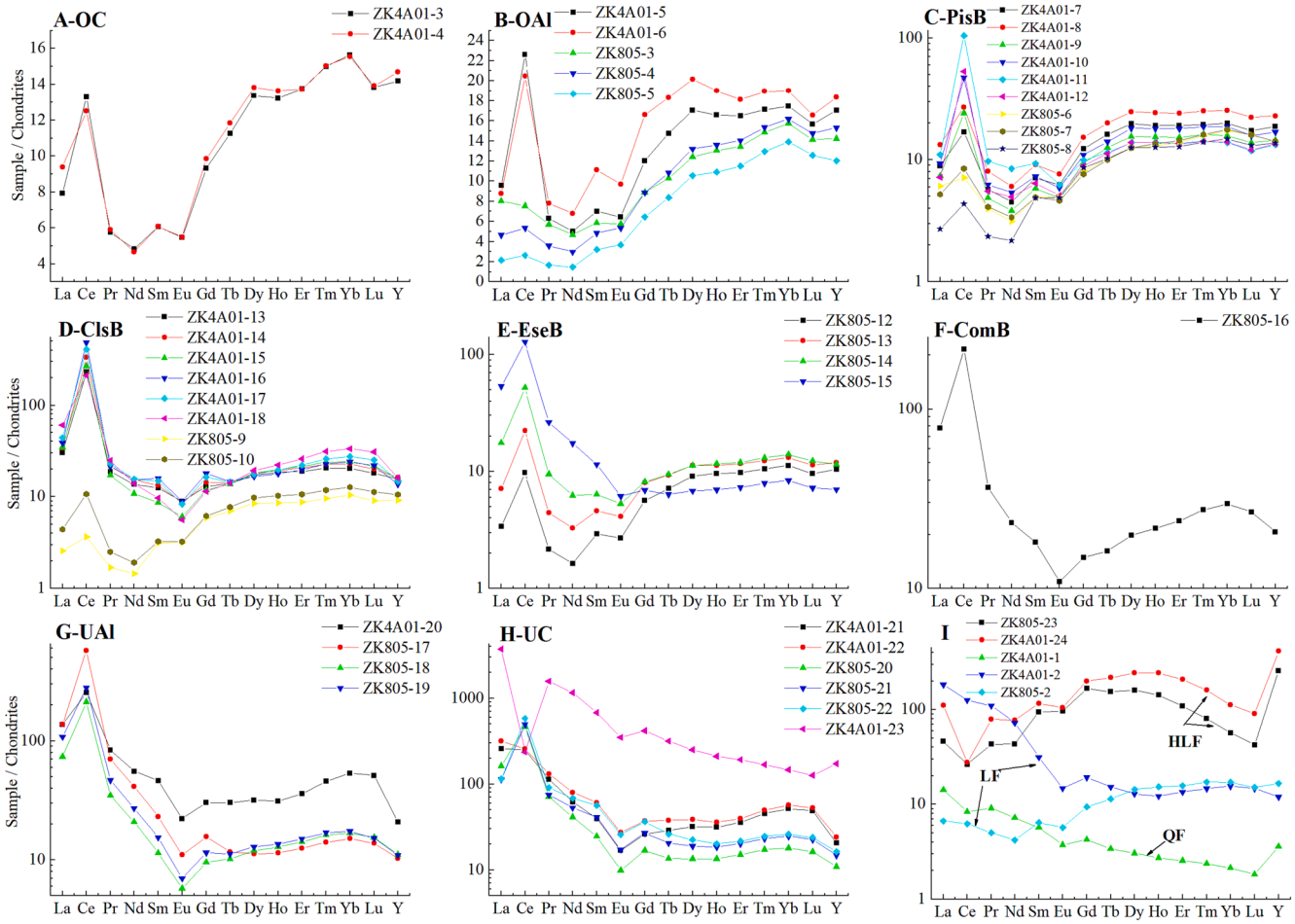

Fig. 9. Chondrite-normalized REE patterns for the different lithologies at Danping. Normalizing values are from (Haskin et al., 1968).

enriched in strong lateritization, especially in the bauxite and kaolinitic bauxite zones (Figs. 6, 12 and 13). It is inferred that Zr is enriched with bauxite formation simultaneously with Al and Ti. Scandium is highly enriched in moderate lateritizaton, and its content is much higher in the laterite and bauxite zones than other zones (Figs. 6, 12 and 13). All LREE and HREE are significantly enriched in weak to moderate lateritization, whereas Y is enriched in moderate lateritization. Therefore, LREE content is much higher in the kaolinitic bauxite zone, and HREE are mostly enriched in the laterite zone, which leads to LREE-HREE decoupling in the ore host (Table 1; Figs. 6 and 13).

Yttrium-bearing minerals (e.g., xenotime) were identified in the bauxite layer (Fig. 4), but not in the footwall or in the HLF transition zone. This is consistent with that xenotime forms mainly in acidic environment, and decomposes readily in alkaline environment (de

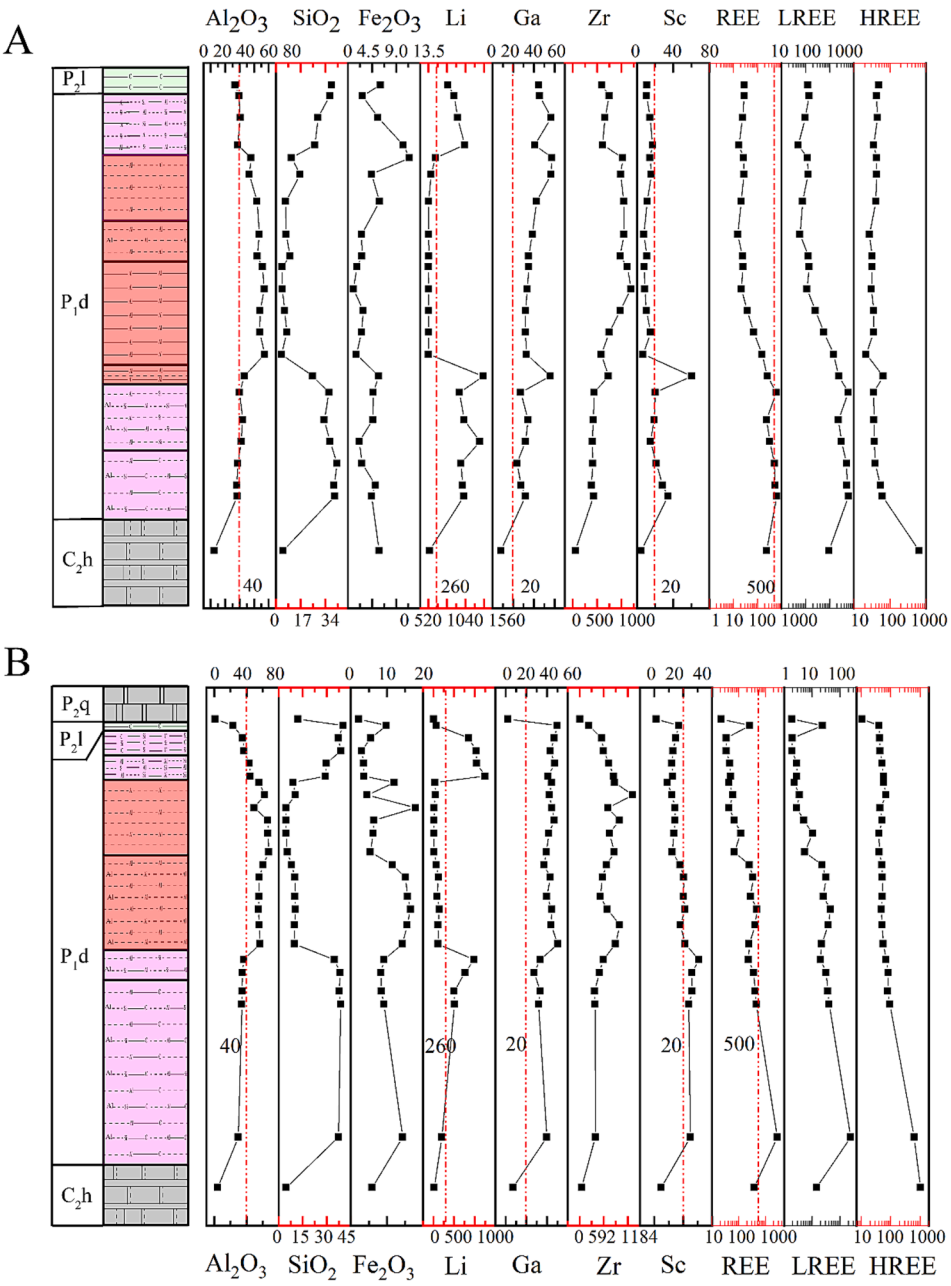

Fig. 10. Variation trends of Al_2O_3, SiO_2, Fe_2O_3, Li, Ga, Zr, Sc, and REE contents across the stratigraphy. (A) ZK805, (B)AK4A01. Unit is wt.% for Al_2O_3, SiO_2 and Fe_2O_3, and ppm for other elements.

Sousa Filho and Serra, 2008; Matraszek et al., 2011). Possible xenotime source in the ore host could be the source rock. However, previous studies have shown that the Hanjiadian Fm. (interpreted ore-material source) has very low Y content (23.8–68.0 ppm) and very few Y-bearing minerals (Gu et al., 2013a; Wang et al., 2013b). The bauxite differentiation and enrichment occurred in an acidic environment with sufficient raw materials, thus the xenotime is more likely to be formed during the bauxite formation. The HLF has low REE content (10.2–31.97 ppm; (Gu et al., 2013a; Jin et al., 2019), yet the HLF in the profiles ZK805 and ZK4A01 shows significant Gd-Lu (146 and 226 ppm, respectively) and Y (501 and 810 ppm, respectively) enrichment, with ΣLREE/ΣHREE <1 (Table 1). This may be caused by that our samples were from the transition zone between the UC and HLF, which enriches HREE. This suggests that HREE may have migrated further in the profiles than LREE.

5.2. *Enrichment mechanism of Li and REE*

Geochemical behavioral differences in critical metals lead to different separation and enrichment processes, and we focus on those of Li and REE. Lithium is enriched in the upper and bottom parts of the ore host, and the middle part is relatively Li-depleted. Meanwhile, REE show a downward increasing trend in the ore host, with the LREE increase higher than that of HREE (Table 1; Fig. 10).

As Fig. 6 implies that the formation of bauxite underwent desilicification, Al- and Fe-enrichment first, and then desilicification, deiron, and Al-enrichment. The bauxite formation in general consists of three main stages: (1) initial enrichment, (2) re-enrichment, and (3) leaching modification (Huang et al., 2014; Liu et al., 2016; Long et al., 2018). REE gradually migrated and concentrated during the successive Al enrichment, desilicification, and deferrization. During this process, acidic conditions may have promoted xenotime formation (de Sousa Filho and

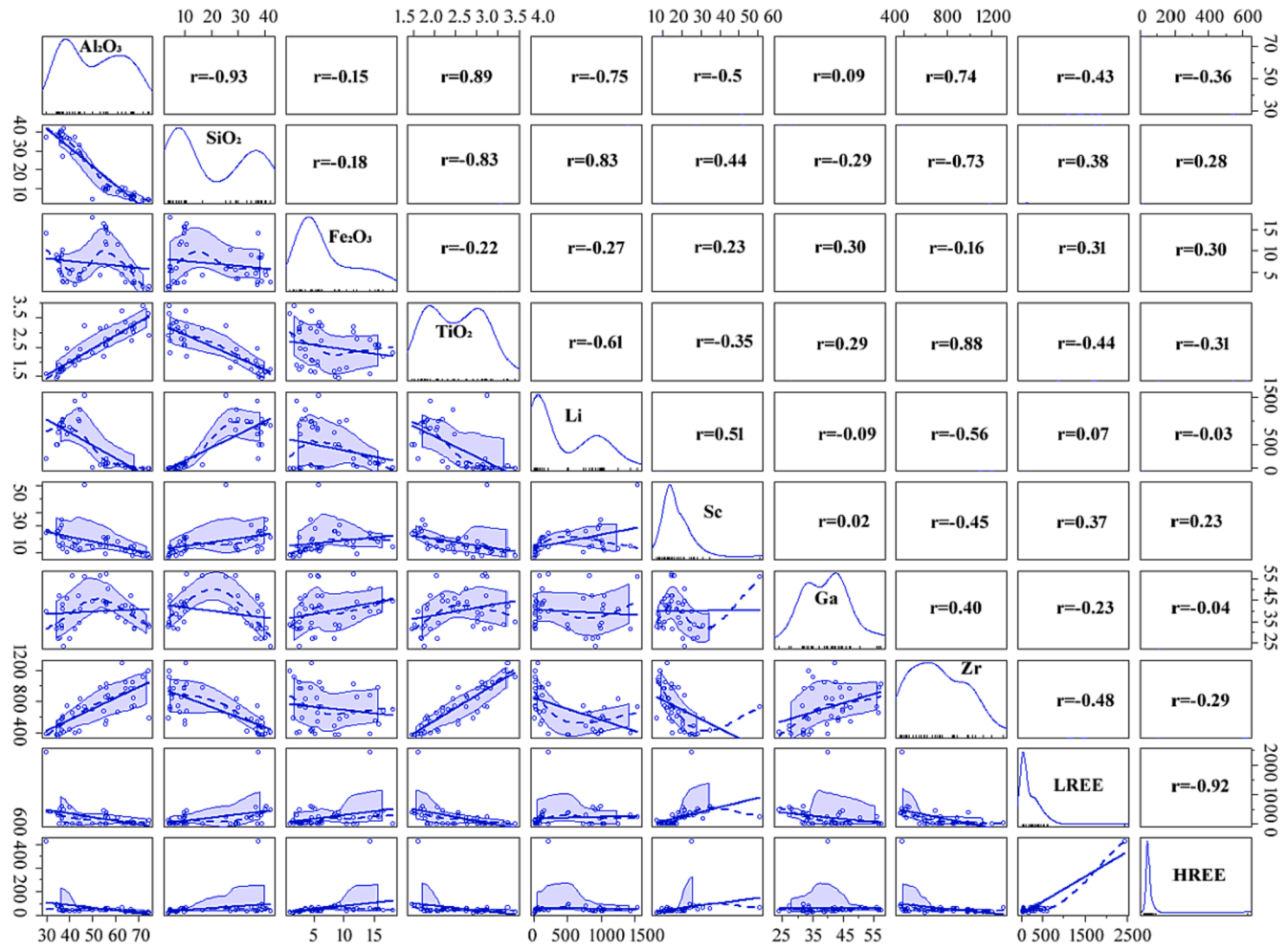

Fig. 11. Scatter matrix plot of various components of the Danping bauxite ore-host series. Kernel density curves and axial whisker plots are shown on the main diagonal. The lower triangles both contain straight-line and smoothed fits, where the solid line is the straight-line fit curve, the dashed line is the smoothed fit curve, and the shaded 95% confidence interval casts are plotted. The upper triangles show the correlation coefficients for the straight-line fits.

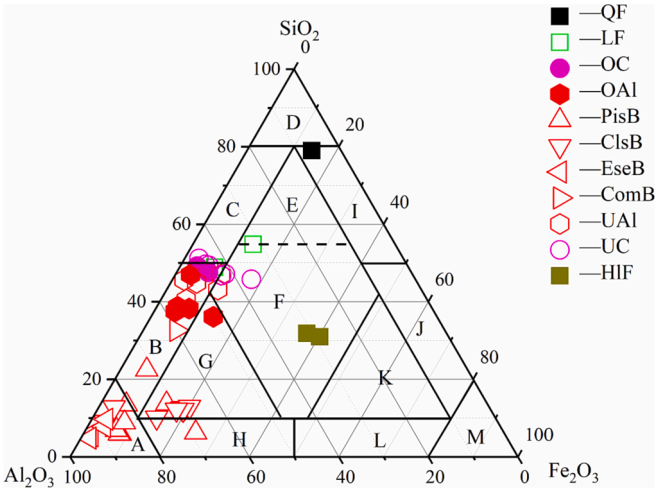

Fig. 12. Ternary Al_2O_3-SiO_2-Fe_2O_3 plot, showing the mineralogical classification of the ore-host series (Aleva, 1994). A-Bauxite, B-Kaolinitic bauxite, C-Bauxitic kaolinite, D- Kaolinite, E- Kaolinite, F-Laterite, G- Bauxite, H-Ferritic bauxite, I-Ferritic kaolinite, J-Kaolinitic ferrite, K-Ferrite, L- Bauxitic ferrite, M—Ferrite.

Serra, 2008; Matraszek et al., 2011), whilst alkaline conditions would promote bastnaesite formation (Johannesson et al., 1996). The discovery of both minerals at Danping indicates complex pH conditions during mineralization consistent with previous reports (Wang et al., 2010). It also suggested that pH changes may have facilitated the REE enrichment from the perspective of rare earth dissolution, fractionation and precipitation (Gu et al., 2013a; Huang et al., 2014).

The initial enrichment (Fig. 14A) occurred in the Late Carboniferous (Chen et al., 2022; Huang et al., 2014; Wang et al., 2013b). The basement rocks were exposed. Under warm and humid climate conditions, the bedrock was weathered to form large amounts of (calcareous) laterite residues, which were deposited in situ or close to the source rocks. Al-minerals were mainly enriched in this process, and the primary minerals were desilicified and Fe-rich to form clay minerals.

This stage is the main Li enrichment stage. Under epigenesis, some Li may precipitate in the solution from host mineral lattice as Li^+ ions, but they were readily adsorbed on clay minerals, due to their large surface area and small size (Huang et al., 2014). It infers that the formation of clay minerals and the transformation between clay minerals are essential for the fractional enrichment of Li (Huang et al., 2014; Ling et al., 2020). The lateritization stage, which favors clay formation, is important for Li-REE enrichment via decomposition of primary Li-/REE-bearing minerals and the later adsorption of these elements onto clay minerals. Some Ce^{3+} may be oxidized to Ce^{4+} and retained in the upper part of the profile, fractionating Ce from the other REE (Elderfield and Greaves, 1982).

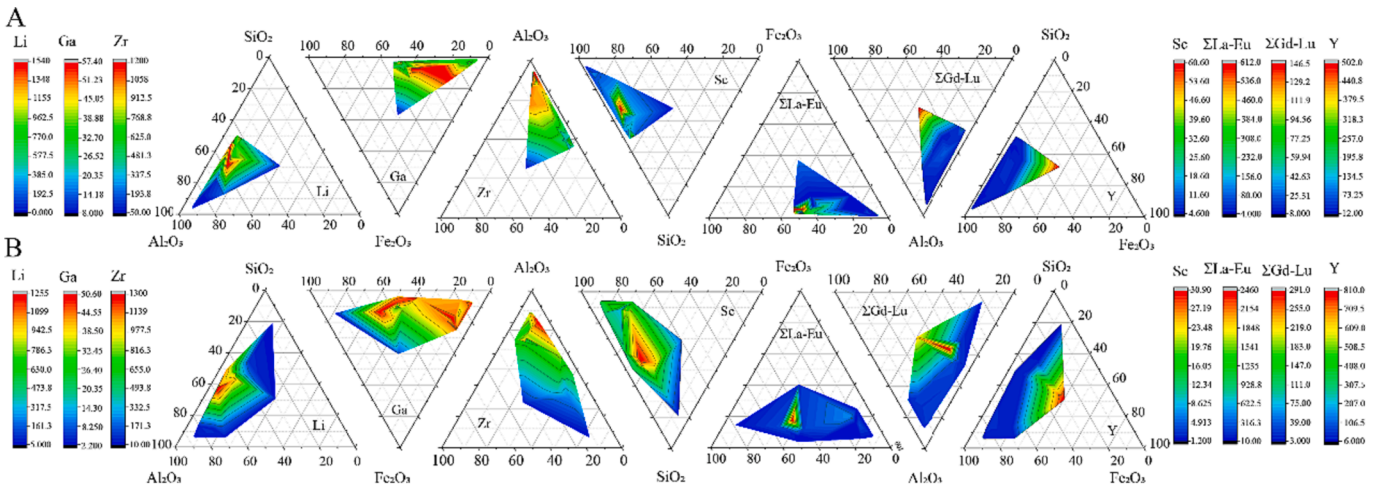

Fig. 13. Distribution diagram of Al_2O_3-SiO_2-Fe_2O_3-Li, Ga, Zr, REE. (A) ZK805, (B) ZK4A01.

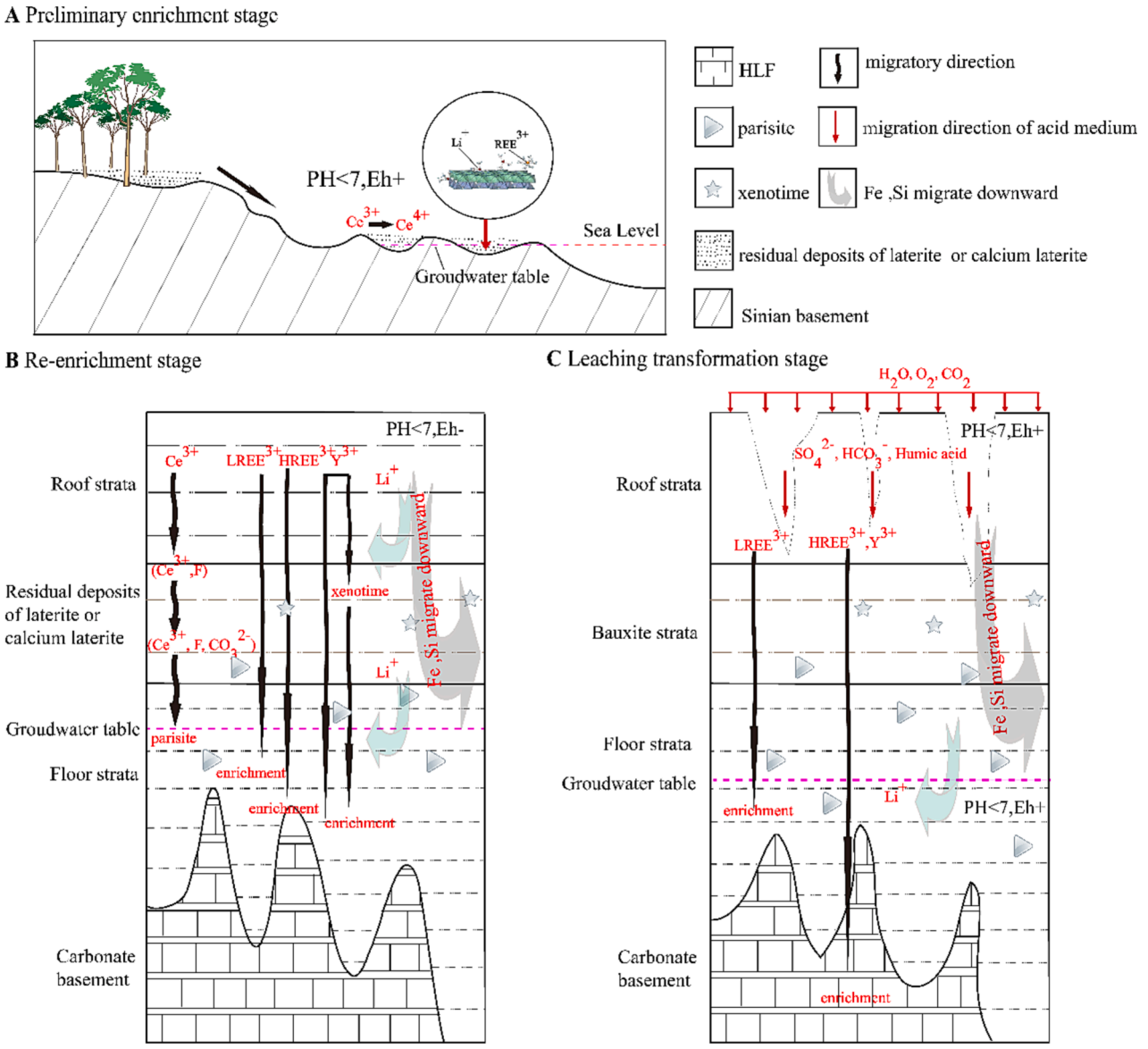

Fig. 14. Schematic diagram of REE enrichment mechanisms in the bauxite-bearing rocks in northern Guizhou.

Table 2
Average concentrations of critical metals and Al_2O_3 in the ore-bearing series (ppm; Al_2O_3 in wt.%), as well as respective total thickness (m).

	Thickness	Al_2O_3	Li	Ga	Zr	Sc	REE
ZK805	3.77						
Overlying bauxitic clay	1.65	39.2	**957**	**34.4**	**488**	18.9	225
bauxite	2.12	63.8	22.5	**39.9**	**931**	12.2	67.2
Underlying bauxitic clay	1.10	——	——	——	——	**22.2**	**479**
ZK4A01	6.50						
Overlying bauxitic clay	3.40	36.5	**710**	**37.7**	**525**	19.3	233
bauxite	3.10	58.8	49.6	**43.1**	**784**	15.8	186
Underlying bauxitic clay	3.05	——	——	——	——	**26.3**	**596**

The re-enrichment stage (Fig. 14B) occurred in the Early Permian (Chen et al., 2022; Huang et al., 2014; Wang et al., 2013b). The seawater flooding may have further acidified and reduced the water column. Li^+ and Li-rich colloidal particles can be further enriched downward as the groundwater level fell, but the Li would not migrate far due to its adsorption on clay minerals or the influence of the diving surface (reduced hydrodynamics or ion saturation increase).

Meanwhile, as the groundwater level fell, the reduced REE-rich acidic leachate percolated downward to the bottom of the profile. Due to the neutralizing effect of alkaline earth metals (e.g., Ca and Mg) in the Huanglong Fm. tuffs and the impermeability of the Hanjiadian Fm. mudstone-shale, the fluid became alkaline and REE precipitated as a result. Meanwhile, Ce^{4+} trapped in the upper part of the profile was converted to Ce^{3+}, and migrated downward to the soil-rock interface, which is also a pH and redox front. With further increase of the fluid Ce^{3+} concentration, it can combine with F^- and CO_3^{2-} to form REE minerals (Huang et al., 2014; Wang et al., 2010; Wang et al., 2013b). Because of the high clay content in the bottom of the ore host (Huang et al., 2014), it could effectively adsorb REE complexes and concentrate REE. Due to the larger ion radii, LREE adsorb on clay minerals more readily than HREE, hence clay-rich bauxite and claystone can better concentrate LREE (Maksimovic and Pantó, 1991; Wang, 1989). The unadsorbed HREE may have continued to migrate downward, some reaching the transition zone of the Huanglong Fm. tuffs and precipitated there. This process may have formed the feature of increasing REE (especially LREE) down depth in the profile.

The leaching transformation stage (Fig. 14C) may have occurred in the Middle Permian (Chen et al., 2022; Huang et al., 2014; Wang et al., 2013b). The crustal may have uplifted and exposed the ore host sequences. This allowed leaching modification, in which organic matter and pyrite were oxidized to form an acidic environment. Li would be lost with continuous desilicification and alumina enrichment, causing its depletion in high-grade bauxite ores. Meanwhile, the acidic environment promoted continuous downward leaching of REE (especially LREE) in fluorine complexes, which fractionated LREE from HREE down the leaching profile.

At a specific temperature and pressure, the fluid Ca^{2+} or CO_3^{2-} activity changes may cause the conversion of fluorocarbons, i.e., $2REE(CO_3)F + CO_3^{2-} + Ca^{2+} \rightarrow REE_2Ca(CO_3)_3F_2$ (Williams-Jones and Wood, 1992). During the downward migration of Y under acidic conditions, Y could combine with the more reactive phosphate rocks and precipitate to form xenotime in the lower part of the bauxite layers (MacLean et al., 1997; Onac et al., 2005). As the environment became more alkaline, xenotime would be redissolved and Y further migrated down the profile. Hence, xenotime is only found in the local bauxite layer at Danping (Fig. 5). Meanwhile, Y may have continued to migrate downward as a complex with Gd-Lu to the lower part of the ore host, and then concentrated in the clay layer or the Huanglong Fm. tuff transition zone, which is more distant than the REE-rich claystone (parisite-rich claystone).

5.3. Economic potential of critical metals in the bauxite ore-host sequence

The Danping bauxite orebody covers an area of ~40 km^2, with a thickness of 3.0–10.0 m (Huang et al., 2014; Jin et al., 2015). The resources of associated Li, Ga, Zr, Sc, and REE in the ore-host sequence are comprehensively evaluated (Table 2). Referring to the standard of associated Li in sand ore (>260 ppm; (Jin et al., 2019)), the bauxitic clay (710–957 ppm) and nearby rock formations meet the comprehensive evaluation requirements. Gallium content (34.4–43.1 ppm) meets the comprehensive evaluation index (0.01–0.002%) in China (MRIRMEC, 2010); Zirconium content meets the industrial recovery index of coastal sand type (>296 ppm; (Huang et al., 2014)), and the ore host (488–931 ppm) meet the comprehensive evaluation requirements; Scandium content meets the foreign industrial recovery index (20–50 ppm; (Jin et al., 2019)), and some ore layers (underlying bauxite clay 22.2–26.3 ppm) meet the comprehensive evaluation requirements. REE distribution in the study area is typical of LREE-enriched type and their content meets the index of weathered crust type REE (REEO: boundary position >0.07%, industrial recovery index), underlying bauxite clay (454–532 ppm) meet the comprehensive evaluation requirements.

The general thickness of the orebody is generally 1/2 to 1/4 of the ore-host sequence, and many places in the ore system remain unexplored (Huang et al., 2014). This implies even greater potential for increasing the critical metal resources.

6. Conclusions

The enrichment of critical metals (Li, Ga, Zr, Sc, and REE) in the Danping bauxite is relatively high, and there are significant differences in the types and enrichment of critical metals in different locations and types of bauxite/rocks. Lithium accumulates in the aluminous rock layer at the top/bottom of the profile, or in the bauxite layer that contains some aluminosilicates. Gallium and Zirconium are enriched in all the bauxite layers. Scandium is enriched in some bauxite layers and basement rocks. REE are mainly enriched in the basement rocks (especially UC), and formed bastnasite and xenotime locally. HREE are also enriched locally in the HLF transition zone. Mechanism shows that during lateritization, the extensive clay formation and the leaching and later adsorption of Li^+ on clay minerals had promoted Li^+ enrichment. With continuous desilicification and alumina enrichment, substantial Li would be lost, leading to the observed Li depletion in high-grade bauxite ores. REE are mainly enriched in the laterite stage, followed by differentiation and re-enrichment under acidic conditions. Meanwhile, alkaline conditions during migration had promoted bastnasite precipitation, forming the REE-rich claystone at Danping. They are enriched above a pH barrier in the lower carbonate plate, with HREE being capable to migrate further than LREE.

Declaration of Competing Interest

The authors declare that they have no known competing financial interests or personal relationships that could have appeared to influence the work reported in this paper.

Data availability

The data that has been used is confidential.

Acknowledgments

We appreciate the assistances of S.Q. Yang in major element analyses, J. Hu, Y. Hang and B. Zhou for trace element analyses, Y. Meng for XRD analyses, W.Q. Zheng and X. Li for SEM analyses. The paper has benefited from constructive comments of two anonymous reviewers. This work is jointly supported by CAS "Light of West China" Program (to H.-P. Fan), the State Key Program of National Natural Science Foundation of China (No. 92162218), and the Guizhou Provincial Science and Technology Support Program (QKHZC[2019]2859).

References

Aleva G.J.J., 1994. Laterites. Concepts, Geology, Morphology and Chemistry. International Soil Reference and Information Centre, Wageningen, the Netherlands. 169.

Bárdossy, G., 1982. Karst Bauxites. Elsevier, Amsterdam.

Bardossy, G.Y., Aleva, G.J.J., 1990. Lateritic bauxites. Elsevier Scientific Publication, Amsterdam.

Chen, P.W., Liu, B., Wang, T.S., Zhou, L.L., Wang, Y.B., Sun, G.T., Hou, K.J., Weng, S.F., Zeng, Q.D., Long, Z., Fu, Y., 2022. Genesis of the Danping bauxite deposit in northern Guizhou, Southwest China: Constraints from in-situ elemental and sulfur isotope analyses in pyrite. Ore Geology Reviews 148, 1–15.

de Sousa Filho, P.C., Serra, O.A., 2008. Tripolyphosphate as precursor for $REPO_4$:Eu^{3+}(RE = Y, La, Gd) by a polymeric method. Journal of Fluorescence 18 (2), 329–337.

Du, L., Tang, Y.Y., Zhang, S.F., Li, Y., Gong, X., Xiang, M.K., Wen, Y.Y., 2022. Critical Metal Enrichments in the Aluminiferous Rock Series in the Bauxite Deposits of Guizhou Province, and their Resource Potential. Acta Sedimentologica Sinica (Network First).

Elderfield, H., Greaves, M.J., 1982. The rare earth elements in seawater. Nature 296 (5854), 214–219.

Gu, J., Huang, Z.L., Fan, H.P., Jin, Z.G., Yan, Z.F., Zhang, J.W., 2013a. Mineralogy, geochemistry, and genesis of lateritic bauxite deposits in the Wuchuan–Zheng'an–Daozhen area, Northern Guizhou Province. China. J. Geochem. Explor. 130, 44–59.

Gu, J., Huang, Z.L., Fan, H.P., Ye, L., Jin, Z.G., 2013b. Provenance of lateritic bauxite deposits in the Wuchuan-Zheng'an-Daozhen area, Northern Guizhou Province, China: LA-ICP-MS and SIMS U-Pb dating of detrital zircons. Journal of Asian Earth Sciences 70–71, 265–282.

Han, Z.H., Wu, B., Weng, S.F., Chen, Q., Tao, P., 2016. Geochemical characteristics of bauxite deposits in the Wuchuan-zheng'an-Daozhen area of Guizhou province and their geological implications. Geology and Exploration 52, 678–687 in Chinese with English abstract.

Hans Wedepohl, K., 1995. The composition of the continental crust. Geochimica et Cosmochimica Acta 59 (7), 1217–1232.

Haskin, L.A., Wildeman, T.R., Haskin, M.A., 1968. An accurate procedure for the determination of the rare earths by neutron activation. Journal of Radioanalytical Chemistry 1 (4), 337–348.

Huang, Z.L., Jin, Z.G., Xiang, X.L., Gu, J., Wu, G., Chen, X., Su, Z., Zhao, Y., Lin, Y., Lin, Z., 2014. Metallogenic Theory and Pridiction of Bauxite Deposites in the Wuchuan Zheng'an Daozhen Area, Northern Guizhou Province. Science Press, Beijing (in Chinese with English abstracts), China.

Jin, Z.G., Dai, L.S., Zhou, J.X., Xie, X., Peng, S., Huang, Z.L., Gu, J., 2015. The distribution of associated elements Li, Sc and Ga in the typical bauxite deposits over the Wuchuan−Zheng'an−Daozhen bauxite ore district, northern Guizhou Province. Geology in China 42, 1910–1918 in Chinese with English abstracts.

Jin, Z.G., Liu, C.S., Zou, L., Zheng, M.H., Zhang, L., Han, Y., 2018. Geochemical Evidence of Sedimentary Environment of Permian Bauxite in the Wuchuan-Zheng'an-Daozhen Area, Guizhou Province. Acta Geologica Sinica 92, 817–827 in Chinese with English abstracts.

Jin, Z.G., Liu, L., Huang, Z.L., Liu, C.S., Zheng, M.H., Gu, J., Zou, L., Wang, L., 2019. Occurrence state, enrichment mechanism and resource potential of rare earth, rare metal and rare-scattered elements in ore-bearing rocks in the Wuchuan-Zheng'an-Daozhen bauxite deposit, Guizhou Province. Acta Geologica Sinica 93, 2847–2861 in Chinese with English abstracts.

Johannesson, K.H., Stetzenbach, K.J., Hodge, V.F., Berry Lyons, W., 1996. Rare earth element complexation behavior in circumneutral pH groundwaters: Assessing the role of carbonate and phosphate ions. Earth and Planetary Science Letters 139 (1-2), 305–319.

Lei, Z., Ling, W., Wu, H., Zhang, Y., Zhang, Y., 2023. Geochemistry and Mineralization of the Permian Bauxites with Contrast Bedrocks in Northern Guizhou, South China. Journal of Earth Science 34 (2), 487–503.

Li, P., Yu, W., Du, Y., Lai, X., Weng, S., Pang, D., Xiong, G., Lei, Z., Zhao, S., Yang, S., 2020. Influence of geomorphology and leaching on the formation of Permian bauxite in northern Guizhou Province. South China. J. Geochem. Explor. 210, 106446.

Ling, K.-Y., Tang, H.-S., Zhang, Z.-W., Wen, H.-J., 2020. Host minerals of Li-Ga-V-rare earth elements in Carboniferous karstic bauxites in southwest China. Ore Geology Reviews 119, 103325.

Ling, K., Wen, H., Fan, H., Zhu, X., Li, Z., Zhang, Z., Grasby, S.E., 2023. Iron Loss During Continental Weathering in the Early Carboniferous Period Recorded by Karst Bauxites. Journal of Geophysical Research-Earth Surface 128, 1–15.

Liu, X.F., Wang, Q., Zhang, Q., Zhang, Y., Li, Y., 2016. Genesis of REE minerals in the karstic bauxite in western Guangxi, China, and its constraints on the deposit formation conditions. Ore Geology Reviews 75, 100–115.

Long, Y.Z., Chi, G.X., Liu, J.P., Zhang, D.X., Song, H., 2018. Uranium enrichment in a paleo-karstic bauxite deposit, Yunfeng, SW China: Mineralogy, geochemistry, transport – deposition mechanisms and significance for uranium exploration. Journal of Geochemical Exploration 190, 424–435.

MacLean, W.H., Bonavia, F.F., Sanna, G., 1997. Argillite debris converted to bauxite during karst weathering: evidence from immobile element geochemistry at the Olmedo Deposit. Sardinia. Miner. Deposita 32 (6), 607–616.

Maksimovic, Z., Pantó, G.y., 1991. Contribution to the geochemistry of the rare earth elements in the karst-bauxite deposits of Yugoslavia and Greece. Geoderma 51 (1-4), 93–109.

Mameli, P., Mongelli, G., Oggiano, G., Dinelli, E., 2007. Geological, geochemical and mineralogical features of some bauxite deposits from Nurra (Western Sardinia, Italy): insights on conditions of formation and parental affinity. International Journal of Earth Sciences 96 (5), 887–902.

Matraszek, A., Radominska, E., Szczygiel, I., 2011. Modified Pechini synthesis of La, Ce, and Pr orthophosphates and characterization of obtained powders. Journal of Thermal Analysis and Calorimetry 103 (3), 813–819.

Onac, B.P., Ettinger, K., Kearns, J., Balasz, I.I., 2005. A modern, guano-related occurrence of foggite, $CaAl(PO_4)(OH)_2{\cdot}H_2O$ and churchite-(Y), $YPO_4{\cdot}2H_2O$ in Cioclovina Cave. Romania. Mineral. Petrol. 85, 291–302.

Qi, L., Hu, J., Conrad, D.G., 2000. Determination of trace elements in granites by inductively coupled plasma mass spectrometry. Talanta 51, 507–513.

Resources Industry Requirements Manual Editorial Committee (MRIRMEC), 2010. Reference manual for mineral industry requirements. Geological Publishing House, Beijing (in Chinese).

Schellmann, W., 1982. Eine neue Lateritdefinition. Geol. Jabrb. Reihe. D 31–47.

Schellmann, W., 1986. A new definition of laterite. Memoirs - Geological Survey of India 1–7.

Sun, Y.Z., Zhao, C.L., Qin, S.J., Xiao, L., Li, Z., Lin, M., 2016. Occurrence of some valuable elements in the unique 'high-aluminium coals' from the Jungar coalfield. China. Ore Geol. Rev. 72, 659–668.

Wang, Z.G., 1989. REE Geochemistry. Science Press, Beijing (in Chinese).

Wang, Q., Deng, J., Liu, X., Zhang, Q., Sun, S., Jiang, C., Zhou, F., 2010. Discovery of the REE minerals and its geological significance in the Quyang bauxite deposit, West Guangxi, China. Journal of Asian Earth Sciences 39 (6), 701–712.

Wang, T., Fu, Y., Chen, P., Hou, K., Tang, B.o., Luo, P., Yao, L., Liu, B., Long, Z., Liu, Y., Liu, G., 2023. Detrital composition and sedimentary provenance of Early Carboniferous Al-bearing rock series in central Guizhou. Ore Geology Reviews 156, 105404.

Wang, X., Jiao, Y., Du, Y., Ling, W., Wu, L., Cui, T., Zhou, Q.i., Jin, Z., Lei, Z., Weng, S., 2013b. REE mobility and Ce anomaly in bauxite deposit of WZD area, Northern Guizhou. China. J. Geochem. Explor. 133, 103–117.

Wang, DengHong, Li, PeiGang, Qu, WenJun, Yin, LiJuan, Zhao, Z., Lei, ZhiYuan, Wen, ShenFu, 2013a. Discovery and preliminary study of the high tungsten and lithium contents in the Dazhuyuan bauxite deposit, Guizhou, China. Science China-Earth Sciences 56 (1), 145–152.

Williams-Jones, A.E., Wood, S.A., 1992. A preliminary petrogenetic grid for REE fluorocarbonates and associated minerals. Geochimica et Cosmochimica Acta 56 (2), 725–738.

Xu, B., Zhang, H.S., Chen, J.P., Wang, Q.F., Yao, M.J., 2017. Geological features and genesis of bauxite deposit in Danping, Guizhou province. Journal of Guilin University of Technology 37, 570–579 in Chinese with English abstracts.

Yu, W., Algeo, T.J., Yan, J., Yang, J., Du, Y., Huang, X., Weng, S., 2019. Climatic and hydrologic controls on upper Paleozoic bauxite deposits in South China. Earth-Science Reviews 189, 159–176.

Zhou, J., Yu, W., Du, Y., Liu, X.u., Wang, Y., Xiong, G., Zhao, Z., Pang, D., Shen, D., Weng, S., Liu, Z., Chen, D., 2022. Journal of Geochemical Exploration Provenance change and continental weathering of Late Permian bauxitic claystone in Guizhou Province. Southwest China. J. Geochem. Explor. 236, 106962.